New Zealand Journal of Geology and Geophysics

ISSN: (Print) (Online) Journal homepage: https://www.tandfonline.com/loi/tnzg20

The geological history and hazards of a long-lived stratovolcano, Mt. Taranaki, New Zealand

Shane J. Cronin, Anke V. Zernack, Ingrid A. Ukstins, Michael B. Turner, Rafael Torres-Orozco, Robert B. Stewart, Ian E. M. Smith, Jonathan N. Procter, Richard Price, Thomas Platz, Michael Petterson, Vince E. Neall, Garry S. McDonald, Geoffrey A. Lerner, Magret Damaschcke & Mark S. Bebbington

To cite this article: Shane J. Cronin, Anke V. Zernack, Ingrid A. Ukstins, Michael B. Turner, Rafael Torres-Orozco, Robert B. Stewart, Ian E. M. Smith, Jonathan N. Procter, Richard Price, Thomas Platz, Michael Petterson, Vince E. Neall, Garry S. McDonald, Geoffrey A. Lerner, Magret Damaschcke & Mark S. Bebbington (2021) The geological history and hazards of a long-lived stratovolcano, Mt. Taranaki, New Zealand, New Zealand Journal of Geology and Geophysics, 64:2-3, 456-478, DOI: 10.1080/00288306.2021.1895231

To link to this article: https://doi.org/10.1080/00288306.2021.1895231

Published online: 17 Mar 2021.

NEW ZEALAND JOURNAL OF GEOLOGY AND GEOPHYSICS
2021, VOL. 64, NOS. 2–3, 456–478
https://doi.org/10.1080/00288306.2021.1895231

Taylor & Francis
Taylor & Francis Group

RESEARCH ARTICLE

OPEN ACCESS Check for updates

The geological history and hazards of a long-lived stratovolcano, Mt. Taranaki, New Zealand

Shane J. Cronin [a], Anke V. Zernack [b], Ingrid A. Ukstins[a], Michael B. Turner[c], Rafael Torres-Orozco [d], Robert B. Stewart[b], Ian E. M. Smith[a], Jonathan N. Procter[b], Richard Price[e], Thomas Platz[f], Michael Petterson[g], Vince E. Neall[b], Garry S. McDonald[h], Geoffrey A. Lerner [a,i], Magret Damaschcke[j] and Mark S. Bebbington[b]

[a]School of Environment, The University of Auckland, Auckland, New Zealand; [b]Volcanic Risk Solutions, Institute of Agriculture and Environment, Massey University, Palmerston North, New Zealand; [c]School of Earth and Environment, Macquarie University, Sydney, Australia; [d]Centre of Geosciences, UNAM, campus Juriquilla, Querétaro, Mexico; [e]School of Science, University of Waikato, Hamilton, New Zealand; [f]LPI, Arizona, USA; [g]Auckland University of Technology, Auckland, New Zealand; [h]Market Economics Ltd, Takapuna, Auckland, New Zealand; [i]Earth Observatory of Singapore, Singapore; [j]British Geological Survey, Nottingham, United Kingdom

ABSTRACT

Mt. Taranaki is an andesitic stratovolcano in the western North Island of New Zealand. Its magmas show slab-dehydration signatures and over the last 200 kyr they show gradually increasing incompatible element concentrations. Source basaltic melts from the upper mantle lithosphere pond at the base of the crust (~25 km), interacting with other stalled melts rich in amphibole. Evolved hydrous magmas rise and pause in the mid crust (14–6 km), before taking separate pathways to eruption. Over 228 tephras erupted over the last 30 kyr display a 1000–1500 yr-periodic cycle with a five-fold variation in eruption frequency. Magmatic supply and/or tectonic regime could control this rate-variability. The volcano has collapsed and re-grown 16 times, producing large (2 to >7.5 km^3) debris avalanches. Magma intrusion along N-S striking faults below the edifice are the most likely trigger for its failure. The largest Mt. Taranaki Plinian eruption columns reach ~27 km high, dispersing 0.1 to 0.6 km^3 falls throughout the North Island. Smaller explosive eruptions, or dome-growth and collapse episodes were more frequent. Block-and-ash flows reached up to 13 km from the vent, while the largest pumice pyroclastic density currents travelled >23 km. Mt. Taranaki last erupted in AD1790 and the present annual probability of eruption is 1–1.3%.

ARTICLE HISTORY
Received 28 June 2020
Accepted 17 February 2021

KEYWORDS
Taranaki; andesite stratovolcano; volcanic hazard; debris avalanche; block and ash flow; Egmont

Introduction

Mt. Taranaki (also known as Mt. Egmont) is the youngest in a NNW-trending chain of volcanoes spanning ~1.75 Ma to present-day, located in the western North Island of New Zealand (Figure 1) (Neall et al. 1986). The 2518 m-high Mt. Taranaki produced eruptives ranging in age from at least 200 ka (Zernack et al. 2011) to ~AD1790 (Lerner et al. 2019a). This volcano is unusual in two ways. Firstly, its erupted compositions have subduction-like signatures (Price et al. 1999), yet its location is difficult to explain in relation to the current New Zealand subduction setting. Secondly, the volcanic edifice regularly collapses to produce large debris avalanches (Zernack et al. 2012), before rapidly rebuilding. The cyclic destruction means that the upper stratovolcano (above ~1200 m) is much younger than composite volcanoes of a similar height (e.g. Ruapehu, Tongariro), and surrounding volcaniclastic deposits comprise ~15 times the volume of the upper edifice (Zernack et al. 2011). The hydrous amphibole-rich andesitic magmas sourced a diverse range of effusive and explosive eruptions (Platz et al. 2007; Turner et al. 2008a). Eruption style variability, coupled with regular cone collapse/reconstruction cycles, has led to a pattern of highly variable frequency and magnitude eruptions over time (Damaschke et al. 2018).

Well described distal volcano-sedimentary deposits and tephra sequences, along with proximal volcaniclastics and lavas show that Mt. Taranaki is an excellent stratovolcano exemplar (Cronin 2013). Its long stratigraphic record provides a series of unique insights into the dynamics of long-lived stratovolcanoes, including: magmatic evolution, edifice stability, magmatic-eruptive cycles and time-varying volcanic hazard. In this paper we review the current state of knowledge of Mt. Taranaki, providing the first review since Neall et al. (1986). Based on information collected over the last 25 years, we synthesise: (1) how Mt. Taranaki relates to current subduction and the active volcanic arc of the Taupo Volcanic Zone; (2) petrological insights into the formation

CONTACT Shane J. Cronin s.cronin@auckland.ac.nz

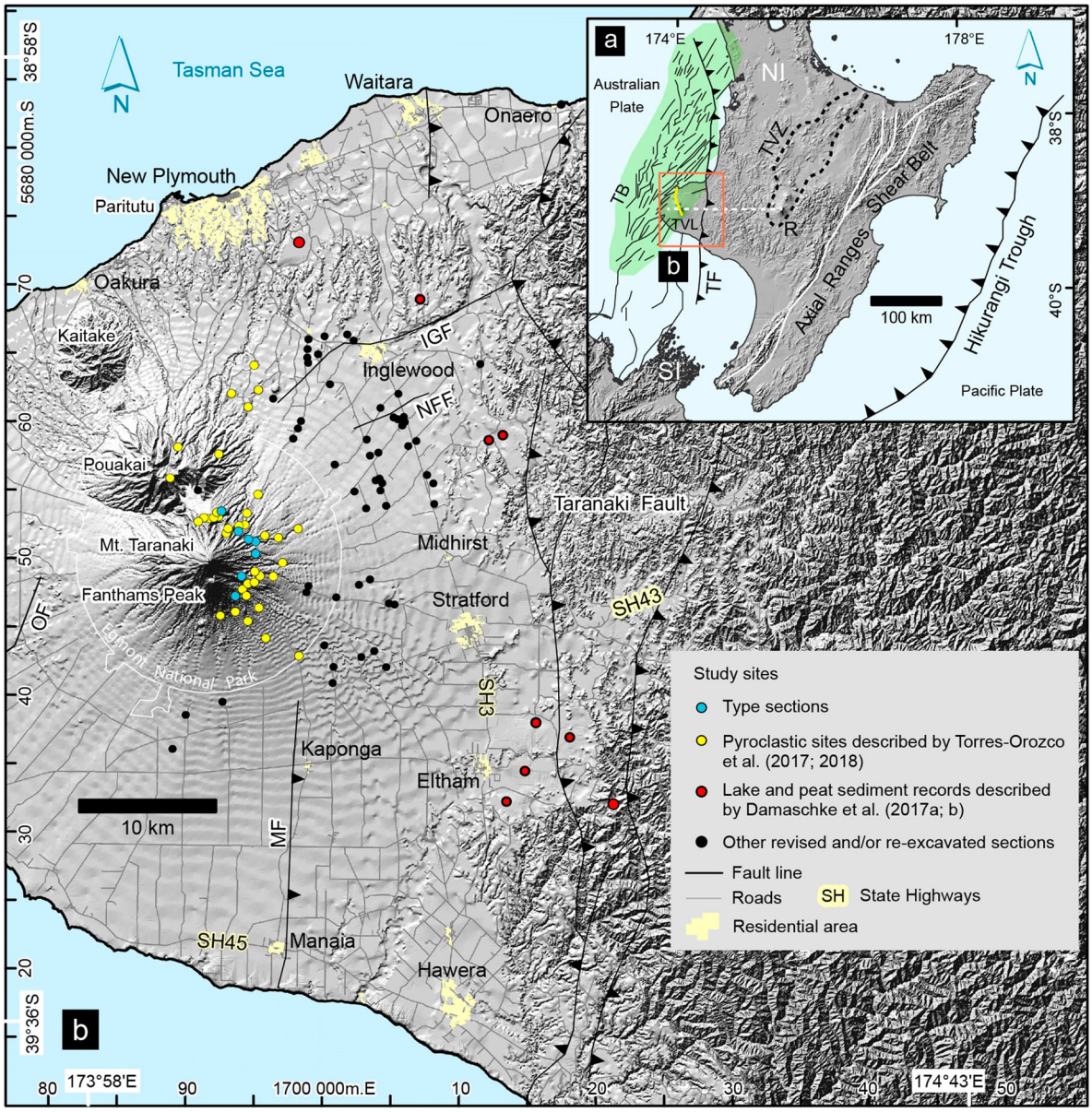

Figure 1. Location map of Mt Taranaki. **A.** Main structural features of the North Island (NI), New Zealand. Mt. Taranaki is located ~140 km west of the Taupo Volcanic Zone (TVZ) and Mt. Ruapehu (R). The Hikurangi Trough marks Pacific Plate subduction beneath the North Island. The Taranaki Basin (TB) is shaded green. The Taranaki Fault (TF) is a Permian crustal-suture. The white dashed horizontal dashed line is the Taranaki-Ruapehu line, marking a transition in crustal thickness. **B.** The Taranaki region, showing the main towns and roads, along with the volcanic structures, and fault zones (IGF, Inglewood Fault; NFF Norfolk Fault; MF Manaia Fault; OF Oanui Fault). Locations of sample sites and core sites are marked.

of Mt. Taranaki magmas; (3) patterns of growth, collapse and evolution of stratovolcanoes; (4) time-varying magmatic-volcanic processes and their relationship to hazard behaviour; and ultimately; (5) what is the current hazard state of Mt. Taranaki? This review concludes by identifying new hypotheses for the drivers of regular or cyclic volcanic behaviour at stratovolcanoes and research avenues to answer open questions about the tectonics of the western North Island.

Geological setting and the origin of Taranaki volcanism

Continental New Zealand straddles the boundary between the Australian and Pacific plates. Current oblique subduction of the Pacific plate begins at the Hikurangi trough, east of the North Island (Figure 1) (Wallace et al. 2004; Reyners et al. 2006; Stern et al. 2006). Moving southward, increasingly oblique motion transitions into transpression on the Alpine Fault along the west coast of the South Island (Norris and Cooper 2007). Taranaki is situated along strike from the change in angle (re-entrant) of the eastern trench from NE-SW to ENE-WSW and lies ~150 km westward of the actively spreading Taupo Rift (and Taupo Volcanic Zone; TVZ), and ~400 km west of the active trench.

The Taranaki volcanic region was used as an example in the seminal paper of Dickinson and Hatherton (1967) that linked K-content of andesitic

magmas to the depth of the subducted slab. Comparing Taranaki to the low-K andesitic volcanism of Ruapehu, Kuno (1966), suggested that deep alkali olivine basalts form at greater distances from a subduction trench, compared to tholeiitic melts at the volcanic front. The current tectonic context of Mt. Taranaki is actively debated and the driving processes for magma formation over the last ~1.75 Ma in this area are poorly understood.

Four geological features play a role in the origin of past and present Taranaki volcanism (Figure 1): (1) the N-S oriented Taranaki Basin; (2) a N-S oriented deep-crustal suture, the Taranaki Fault Zone, east of the volcano; (3) the E-W Taranaki-Ruapehu line that marks a change in crustal thickness; and (4) the subducting Pacific plate slab that includes the leading edge of the Hikurangi Oceanic Plateau (Reyners et al. 2011).

Mt. Taranaki is located within the Taranaki Basin, a sedimentary basin containing up to 6 km of unconsolidated water-saturated Cretaceous-Cenozoic sediments (King and Thrasher 1996). Near Mt. Taranaki, the western margin of the basin is marked by the Cape Egmont Fault Zone, while the eastern boundary is marked by the Taranaki Fault Zone. Below these, Mortimer et al. (1997) identified a basement of diorite, gabbro, granitoid and metamorphic rocks of the Permian-Cretaceous Median Batholith. This abuts the Brook St. Terrane (a Permian arc) ~10 km east of Mt. Taranaki. Around 30 km east of the volcano, a suture zone between the Brook St. Terrane and the volcaniclastic sandstones of Murihiku Terrane is marked by the N-S striking, Taranaki Fault (Figure 1). The fault is seismically detected to the base of the crust (Sherburn et al. 2006) and represents a thrust zone ~8–10 km wide, that has accommodated over 15 km of dip-slip displacement over the last ~80 Ma (Giba et al. 2010).

The Taranaki Basin is ~350 km-long and up to 120 km-wide (Figure 1). It has a history of both extension and compression (Knox 1982; King and Thrasher 1992, 1996). Initial lithospheric extension and subsidence occurred during the Lower Eocene–Upper Oligocene (30–25 Ma). Back-arc extension began coincidentally with subduction initiation 500 km to the east (Stern and Holt 1994). During the Lower Miocene (21 Ma), intra-plate clockwise rotation, around an axis near present Taranaki, coupled with compressional Alpine Fault motions, led to shortening and thrust faulting along the Taranaki Fault zone, locally thickening the crust from ~25 km to >40 km (Holt and Stern 1994; Stern et al. 2006). In the Mid Miocene-Pliocene (12-4 Ma) extension propagated from north to south and was associated with voluminous offshore volcanism. Gravity and magnetic surveys show a series of NNE-SSW-trending back-arc rifts containing large mafic intrusions capped by volcanic edifices (King and Thrasher 1996; Stern et al. 2006; Giba et al. 2010). Each edifice represents a large, long-lived composite medium-K basaltic/andesitic volcanic system (e.g. Morley 2018). Magmas are associated with the leading edge of subducting Pacific plate reaching a dehydration depth (~100–150 km) beneath the Taranaki Basin (King and Thrasher 1996). The migration of rifting, and alternating extension/shortening followed a clockwise rotation of the eastern Taranaki Basin relative to a rigid western block (Stern et al. 2006). Southward migration of volcanism was gradual and likely related to slab rollback, with a 10° steepening of the slab (Giba et al. 2010). A pause in back arc extension in the Taranaki Basin in the Pliocene is attributed to the southern termination of subduction in southern North Island (Stern et al. 2006; Giba et al. 2010). Back-arc extension was then transferred north-eastward, initiating the Taupo Rift. Once the Taranaki Basin extension ceased, associated back-arc volcanism stopped. The most recent and southernmost expression of volcanism in the Taranaki Basin is the <1.75 Ma subaerial Taranaki Volcanic Lineament. This differs to earlier episodes, because there is little or no rifting, and the migration of volcanism is slow, lagging behind the propagation of normal faulting, which is now at least 80 km farther southward (Giba et al. 2010).

Along with basin evolution, broader regional changes within the North Island formed a curved boundary that separates thinner crust (~25 km) within N-NW North Island and thicker crust (~35 km) in S-SE North Island. Part of this boundary, known as the *Taranaki-Ruapehu line*, tracks west-east between Mts. Taranaki and Ruapehu (Sherburn and White 2005; Stern et al. 2006). The crustal transition spans ~8 km across the line, but it has no topographic expression (Salmon et al. 2011). It is thus is interpreted as a dynamic feature, resulting from ongoing convective removal of mantle lithosphere from the western North Island, possibly associated with crustal delamination (Salmon et al. 2011; Dimech et al. 2017). Crustal thinning is compensated by inflow of low density upper mantle material (Stern et al. 2006; 2013).

The post-1.75 Ma Taranaki Volcanic Lineament formed during an absence of basin extension, coupled with an advanced roll-back of the Pacific plate slab. The present subducting Pacific Plate lies at ~120 km below Mt. Ruapehu. Projecting along the Taranaki-Ruapehu line (~40° anticlockwise from the general slab dip) the slab gradually deepens to ~200 km, until it reaches the Taranaki Fault Zone (Reyners et al. 2006; Stern et al. 2006). Up to this point, the slab comprises the ~40 km-thick Hikurangi Plateau, but in front of this lies normal oceanic crust, which steepens to a sub-vertical dip and slab-earthquakes disappear at ~260 km depth (Reyners et al. 2006;

2011; Eberhart-Phillips et al. 2013). Directly below the deepest slab earthquakes, rare earthquakes at 600 km depth may represent a horizontal surface, such as a foundered detached slab (Boddington et al. 2004).

In contrast to the current TVZ, there is no evidence of mantle wedge return flow in the Taranaki region. It may be blocked by the thick upper plate along the Taranaki Fault zone (Reyners et al. 2006), which hinders magma generation via slab-fluid fluxing of the mantle. However, a discrete zone of mantle inflow occurs from the northwest at ~65 km depth below Mt. Taranaki (Reyners et al. 2006). This could be a source of fertile mantle material for magma generation, because it has already been modified during Miocene-Pliocene subduction. Other suggestions of magma generation including mantle flow around the southern edge of the subducting Pacific plate, or through NW-SE oriented tears within the subducting slab (Reyners 1983; Price et al. 1992), are not supported by recent geophysical data (Reyners et al. 2006).

Stern et al. (2006) propose an alternative magma generation model for the post-1.75 Ma volcanism. They suggest that a lithospheric mantle instability (cf., Elkins-Tanton and Grove 2003; Elkins-Tanton 2007) formed below the Taranaki Fault Zone. As mantle material founders, it dehydrates and flux-melts highly metasomatised (K-rich) mantle material above. Fertile mantle material inflow from the northwest (Reyners et al. 2006) could replace the descending lithosphere. South of the Taranaki-Ruapehu line, the crust is much thicker, reducing the opportunity for magmatism. The slab beneath Mt. Taranaki is very steep to sub-vertical (Reyners et al. 2006; 2011), and (Stern et al. 2013) suggested that descending mantle lithosphere could be sliding down it. Countering this model, Giba et al. (2010) considers that there is insufficient space for lithospheric gravitational instability below the Taranaki Fault. This depends on whether the 600 km-deep earthquakes beneath Taranaki represents the front of descending mantle, or a detached and foundering flat-lying slab. Recently, Dimech et al. (2017) suggested that the crust is also delaminating since 5 Ma, rolling from the north along the Taranaki-Ruapehu line and coupled with lithospheric mantle foundering. A several million year delay occurs between crustal delamination and initiation of high-K volcanism in other cases (Elkins-Tanton and Grove 2003). Sporadic high-K volcanism occurred in the western North Island from 3.8 to 1.8 Ma (Briggs 1986), but this was followed by persistent, larger volumes of high-K volcanism along the Taranaki Volcanic Lineament from at least 1.75 Ma (Neall et al. 1986). A 30 mm/yr north to south migration of volcanic centres of the Taranaki Volcanic Lineament is consistent with a magma source progressing southward toward the present position of the Taranaki-Ruapehu Line (Dimech et al. 2017).

Heat flow in the Taranaki region ranges between 40 and 90 mW/m^2 (on average 59 mW/m^2; Kroeger et al. 2013), which is only one tenth of the maximum within the TVZ (700–800 mW/m^2) (Stern et al. 1987). There are no currently active fumaroles, but there are warm and cold springs with mineralised waters (Allis et al. 1995). A region of high heat flow is located north of Mt Taranaki. Its source has been modelled as either a mid-crustal body, ~500 m thick, that intruded over the last 0.5-0.3 Ma, or ~5 km of crustal underplating over the last 2–4 Ma (Allis et al. 1995; Funnell et al. 1996). Its location is consistent with the influx of mantle flow from the northwest seen on seismic tomography (Reyners et al. 2006).

Present-day seismicity and principal stress directions in eastern Taranaki are consistent with a continuation of TVZ back-arc extension (Sherburn and White 2006). East of Mt. Taranaki, strike-slip and normal earthquakes are deep (>25 km), left-lateral transtensional events, associated with the Taranaki-Ruapehu line (Sherburn and White 2005). Geodetically modelled east-west extension across the Cape Egmont Fault Zone west of Mt Taranaki is estimated at ~1 mm/yr (Wallace et al. 2004). West of Mt. Taranaki, earthquakes are 15–25 km-deep and occur in swarms of right-lateral strike slip or normal earthquake motions (Sherburn and White 2005). The western earthquake focal mechanisms and principal stresses are explained by east-west compressive stress related to magma intrusion along a N-S oriented dyke system beneath Mt. Taranaki (Sherburn and White 2006). Such an intrusion would induce long-term stress changes west of the volcano, suppressing normal faulting. Sherburn and White (2006) suggest that eruptions that empty dykes may release stress and induce normal-faulting earthquakes. Pre-historic fault offsets recorded on faults southeast and northwest of Mt. Taranaki, are coincident with large eruptions (e.g. Oanui Fault normal 5 m-displacement over 6.5 ka; and Inglewood fault oblique-normal 3 m-vertical displacement over 13 ka; Hull 1994, 1996). However, for magma to rise in this stress regime, it must overcome compression, and is more-likely to induce thrusting and transpressive/tensional tendencies.

The Taranaki Volcanic Lineament and Mt. Taranaki

The Taranaki Volcanic Lineament (TVL) is a chain of andesite volcanoes, decreasing in age from northwest to southeast: Paritutu, incorporating the Sugar Loaf Islands (1.75 Ma); Kaitake (575 ka), Pouakai (210–250 ka); and Mt. Taranaki (<200 ka) (Figure 1) (Neall et al. 1986: Price et al. 1999; Zernack et al. 2012). The oldest deposits of Mt. Taranaki are debris avalanche deposits with an estimated age of ~200 ka (Zernack et al. 2012).

Paritutu volcano comprises Paritutu Rock (156 m above sea level) and seven Sugar Loaf Islands within a roughly 2.5 km-diameter circular area. These are the eroded remnants of dykes, plugs, and volcanic necks composed of hornblende-andesite (Neall 1979). Seismic reflection, a gravity anomaly (170 g.u.), and an aeromagnetic anomaly (100–130 nT) show that the surface outcrops sit above a 3–4 km-diameter cylindrical intrusive complex extending to ~6 km-depths (Hunt and Syms 1975; Locke et al. 1993; 1994). Paritutu is offset to the east by ~9 km from the three younger edifices of the TVL, the centre-points of which define a NNW (330°) trend. Kaitake, a 684 m high edifice, comprises a highly eroded central zone, 6 km in diameter, which hosts hornblende andesite and diorite dykes. The volcano was once larger, with its outer flanks buried by at least 270 m-thick volcaniclastic deposits from the younger volcanoes (Neall 1979; Gaylord et al. 2014). Its gravity (240 g.u.) and aeromagnetic (500 nT) anomalies indicate an ~85 km^3 intrusive complex at least 3.5 km in diameter that extends ~6 km below the edifice (Hunt and Syms 1975; Locke et al. 1993; 1994). The 1222 m high Pouakai Volcano is centred 9.5 km southeast of Kaitake, and is also deeply eroded and partly buried. The residual volcano is at least 14 km in diameter and comprises hornblende andesite and augite-basaltic andesite lavas (Neall et al. 1986). The gravity (350 g.u.) and aeromagnetic (1100 nT) anomalies associated with Pouakai are much larger than the older volcanoes, indicating a stock of ~150 km^3 extending up to 10 km deep, similar to that of Taranaki (1480 nT) (Locke et al. 1993; 1994; Locke and Cassidy 1997).

Mt. Taranaki at 2518 m is the second-highest peak of the North Island. The edifice above 1400 m-elevation has a volume of ~12 km^3 (Zernack et al. 2012; Zernack et al. 2012). The brittle-ductile transition zone beneath the volcano lies at ~10 km depth, with a low velocity seismic zone present at deeper levels (Sherburn and White 2005). A ~5 km diameter zone below the volcano that extends to 10 km depth, shows high Vp and low Vp/Vs, and is interpreted as mainly solidified intrusive rock (Sherburn et al. 2006).

The main eruptive vent of Mt. Taranaki over the last ~14 ka was the present day summit crater (Torres-Orozco et al. 2017) (Figure 2). The otherwise highly symmetrical composite cone is disrupted by a major parasitic cone, Panitahi/Fanthams Peak (1952m), which has existed for at least 7 ka (Neall et al. 1986) (Figure 2). Panitahi is not oriented along the 330° trend of the TVL, but lies almost due south of the summit, forming a N-S axis between the two main vents of Taranaki Volcano. Other satellite vents are monogenetic. Four flank lava domes occur (Neall 1971): one pair on the northern flanks (Skinner Hill and The Dome) are oriented N-S; while the second vent pair are on the southern edifice flanks (the Beehives) also on a N-S trend. One further eroded vent is identified, the Curtis Ridge spatter cone, on the saddle between Panitahi and the south-eastern flanks of the summit cone (Turner et al. 2008a).

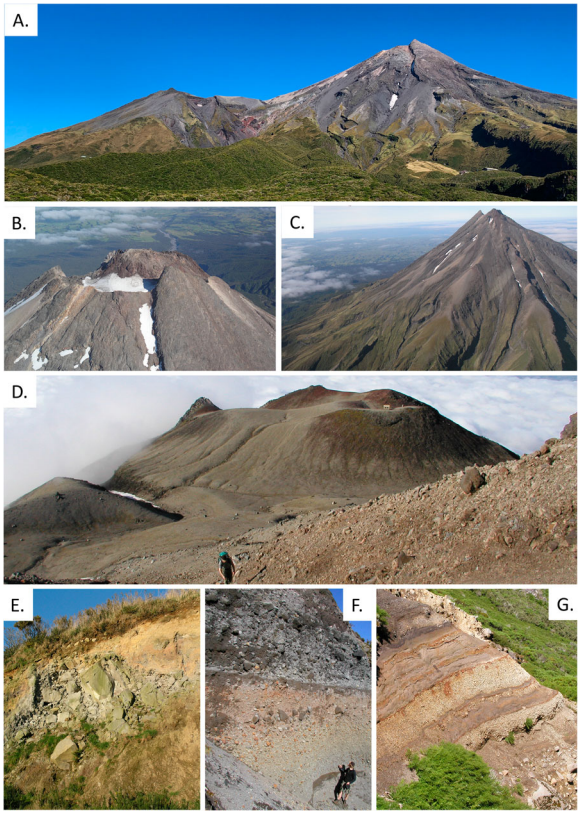

Figure 2. Photos of Mt. Taranaki and deposits. **A**. View from the east, with the 1952 m Panitahi (Fanthams Peak) to the south (left), with the summit cone at 2518 m asl. Note the thick lava ridge-forming lava bluffs in the right foreground. **B**. View into the summit crater from the east, with a crater rim formed by lava flows (<700 yrs old) and the AD1790 lava dome forming the summit (Lerner et al. 2019a). **C**. Northern flanks of Mt. Taranaki showing thin, valley fill lava flows with distinctive levees. **D**. View south to Panitahi cone (Fanthams Peak), dominated by lava spatter. In the right foreground is a pumice-rich pyroclastic density current deposit formed during the AD1655 Burrell eruption episode (Platz et al. 2007). **E.** Typical lava-dominated clast domain (grey) within the Opua Debris Avalanche (7.5 ka BP) on the southern ring plain. The field of view in this image is 20 m wide. **F.** Typical dome-collapse block-and-ash (BAF) deposits that formed during the Maero Eruptive Period during the last ~800 yrs (Lerner et al. 2019a; Lerner et al. 2019b; Lerner et al. 2019c). **G**. Pyroclastic deposits on the SE flanks of the volcano, the prominent pale yellow pumice bed in the centre of the view is a 0.8 m-thick fall phase of the 3.3 ka BP Upper Inglewood eruption episode (Torres-Orozco et al. 2017; 2018).

Above ~1400 m-elevation, Mt. Taranaki is dominated by andesitic lava flows, with a range of morphologies, including short, thick (>30 m) coulees, and up to ~3 km-long blocky lava flows with prominent levees and ponded zones within valleys (Figure 2). Multiple radiating flows descend from both the summit

and Panitahi. Secular paleomagnetic studies (Downey et al. 1994) and tephrostratigraphy indicate that the lavas are <10 ka. Two periods of growth are indicated by paleomagnetizm; a series between 7000 and 2800 yrs and a younger suite aged between 700 and 400 yrs. The youngest set of flows radiate out from the uppermost summit crater rim. Stacks of multiple thin (<10 m) flows with similar compositions occur in many sectors, with paleomagnetic evidence showing that each sequence accumulated rapidly (Downey et al. 1994). The summit hosts a half-sectioned lava dome, formed by a steep, collapsed western flank, along with a crater basin around the remaining sides (Platz et al. 2012). This lava dome formed during the last known eruption of Mt. Taranaki, at AD1790 ± 10 yrs (Lerner et al. 2019a). At ~1400–1500 m, a slope-break occurs and a series of very thick lava flows (50–100 m) form prominent ridges with tephra cover beds indicating ages of >5000 to <14000 yrs B.P. (Figure 2) (Turner et al. 2011a; Torres-Orozco et al. 2017). Lavas pass downslope into volcaniclastic sediments, distributed in a radial drainage network to form a ring plain.

Petrology and geochemistry of Mt. Taranaki eruptives

Mt. Taranaki has erupted basalt, basaltic-andesite and andesite compositions (Figure 3). Published studies have focused mainly on cone lavas (<10 ka) (Price et al. 1992, 1999; Stewart et al. 1996), lava clasts within debris avalanche deposits (<200 ka) (Zernack et al. 2012), and xenoliths within lavas (Gruender et al. 2010; Price et al. 2016).

Taranaki lavas range from vesicular, red and black scoria through non-vesicular to holocrystalline, porphyritic basalt, basaltic andesite and hornblende-andesite lavas (Neall et al. 1986; Price et al. 1992, 1999; Zernack et al. 2012). Most rocks contain 20 to 55% phenocrysts (up to 70% in some andesites). Phenocrysts are typically 0.5–0.8 mm long, rarely up to 3 mm-long and very rarely hornblende can be several cm in length. Glomerocrysts (up to 5 mm-diameter) are common and comprise clinopyroxene, titanomagnetite, plagioclase and olivine, with lesser orthopyroxene and amphibole.

Basalts contain phenocrysts of plagioclase, clinopyroxene, titanomagnetite and olivine in a groundmass of brown, cryptocrystalline glass with microcrystalline plagioclase, clinopyroxene and titanomagnetite ± olivine ± orthopyroxene. Apatite is a common accessory phase and hornblende and orthopyroxene are minor constituents, with phlogopite very rare (Gow 1968; Neall et al. 1986; Stewart et al. 1996; Zernack et al. 2012). Basaltic andesites are petrographically similar to the basalts but span two end memberw from pyroxene-basaltic andesites to amphibole-basaltic andesites (the latter containing up to 30% amphibole). The andesites are dominated by plagioclase and amphibole with <20% of samples containing significant modal clinopyroxene. Higher-silica andesites, (e.g. the summit dome) also contain biotite in a groundmass of cryptocrystalline (<0.05 mm), plagioclase, pyroxene and titanomagnetite.

In all lavas, plagioclase (10–40% of the phenocrysts) shows strong oscillatory zoning, along with sieved-textured cores, resorption zones as well as normal and reverse zoning. Cores range from An_{90} to An_{55} and rim compositions extend to An_{30} (Stewart et al. 1996). In basalts and some basaltic andesites, clinopyroxene and plagioclase are in similar proportions and clinopyroxene shows both sector and oscillatory zoning with higher Mg cores and Fe-rich rims. Clinopyroxene Mg#s (mol. Mg/ Mg + Fe) vary from 0.69 to 0.87 (Stewart et al. 1996; Price et al. 1999; Zernack et al. 2012). Clinopyroxene is closely associated with iron oxide, which is also common as inclusions in olivine, clinopyroxene and plagioclase (Zernack et al. 2012).

Iron oxide is ubiquitous in all rock types and is predominantly titanomagnetite (ulvöspinel with 3–10% wt.% TiO_2) comprising 5–10% of phenocrysts and exhibiting variable degrees of solid state exsolution (Turner et al. 2008b). Chrome spinel occurs as inclusions in olivine and as discreet groundmass grains (Neall et al. 1986). Ilmenite is rare.

Amphibole (0–20% of phenocrysts) commonly has reaction rims of microcrystalline titanomagnetite and clinopyroxene, with variable thickness. Completely pseudomorphed amphibole crystal shapes are also common. Most amphibole is pargasitic with rare grains of magnesiohastingsite or edenite (classification of Leake et al. 1997). Amphibole crystals show Mg-Fe zoning, but core and rim compositions differ in Al_2O_3 and TiO_2 concentrations (Zernack et al. 2012). Olivine is normally zoned and compositions vary in the range Fo_{86-61}. Orthopyroxene in most Taranaki basaltic rocks occurs as rare, crystals up to 5 mm-long mantled by clinopyroxene (En_{74-79}), and as a minor component in glomerocrysts and groundmass (En_{60-66}) (Stewart et al. 1996; Zernack et al. 2012).

Groundmass assemblages are dominated by plagioclase, titanomagnetite and clinopyroxene and interstitial glass, with rare olivine, orthopyroxene, amphibole, phlogopite and apatite. Groundmass glass compositions range from 52 to 75 wt.% SiO2, with slightly higher values in glass inclusions (58 to 76·5 wt.% SiO2) within hornblende and clinopyroxene phenocrysts (Zernack et al. 2012).

Panitahi (Fanthams Peak) lavas are distinct in petrology and composition from the Taranaki summit sourced flows. They are largely porphyritic (40–50% crystals) basaltic andesites (Price et al. 1992) with small phenocrysts (<0.5 mm). They

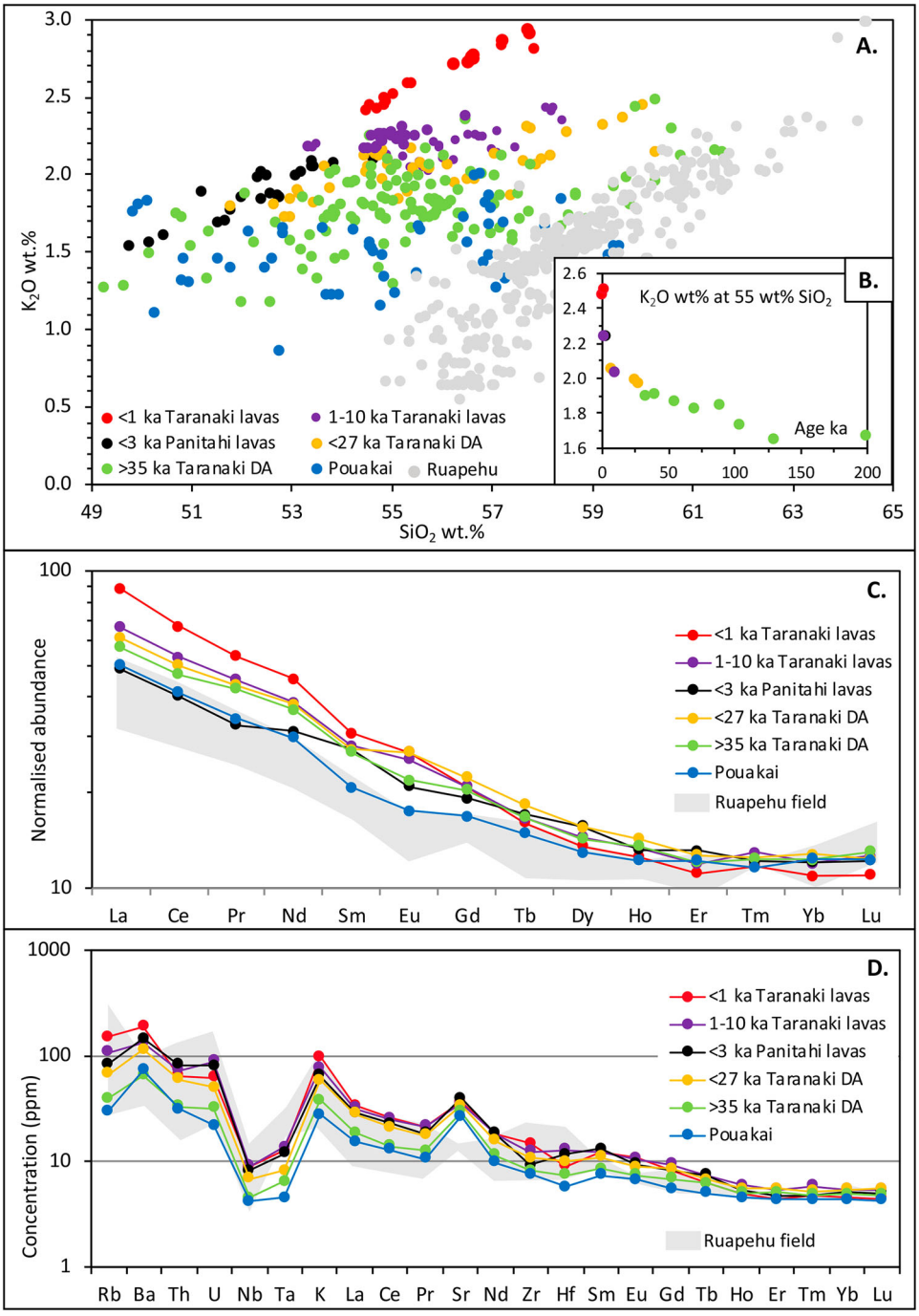

Figure 3. Summary chemical plots for Mt. Taranaki and comparative rock suites (data from Price et al., 1992; 1999; 2005; 2021; Zernack et al. 2012). **A**. K_2O vs. silica plot of Taranaki rock suite, compared to Pouakai and Ruapehu volcanoes. **B**. K55 plot, showing the K_2O wt% at 55% silica content of each dated rock suite from cone and debris avalanche deposits. **C**. Chondrite-normalised Rare Earth Element (REE) plot for a subset of Taranaki andesites, including summit lavas (<1 ka), Panitahi (Fanthams Peak) lavas, debris avalanche (DA) hosted rock from young and old ring plain deposits, compared to Pouakai and Ruapehu volcanoes. **D**. Trace element abundances for a subset of Taranaki andesites, compared to Pouakai and Ruapehu suites.

contain higher contents of olivine (10–20% of phenocrysts), but are dominated by either clinopyroxene, titanomagnetite or plagioclase with rare hornblende. Other textural features are similar to the summit cone lavas.

Xenoliths within Taranaki lavas and pyroclastics are common and include hornfels, amphibolitic gneiss, garnet gneiss and granite-granodiorite sourced from the underlying Median Batholith basement, along with shallow sediments and subvolcanic intrusive lithologies, including gabbro and related cumulates (Gruender et al. 2010; Price et al. 2016).

Older (pre-100 ka) compositions include a greater proportion of more primitive basalts and basaltic andesites than cone lavas (Zernack et al. 2012). Overall the Taranaki lavas are chemically classified as mainly high-K basaltic andesites and andesites (Figure 3). They show relatively low Mg numbers [mol. MgO x 100/(mol. MgO + mol. FeO)] (<52; Price et al. 1992) and low Ni and Cr contents (<40 and 100 ppm,

respectively), which indicate that even the most primitive erupted compositions are not primary melts. The least evolved magmas are modelled by Stewart et al. (1996) and Price et al. (1999) as starting as silica undersaturated, hydrous, large ion lithophile element (LILE)-rich high-Mg basalts. Initial fractionation involved olivine and chromite, followed by clinopyroxene and titanomagnetite in the upper mantle (Figure 4), resulting in high-Al basalts. Basaltic andesite lavas contain dunite, wehrlite and pyroxenite xenoliths, sourced from depleted upper mantle, whereas the andesites contain only lower crustal xenolith suites (Gruender et al. 2010). The second fractionation stage occurs as more evolved magmas assimilated mafic cumulates or mushes at the base of the crust (Figure 4). High-K (up to 6 wt.% K_2O) rhyolitic-trachytic glass, found within lower crustal xenoliths (meta-hornblende pyroxenite, olivine hornblende pyroxenite) are evidence for this fractionation step (Gruender et al. 2010). A third stage occurs as magmas rise through the crust and fractionate clinopyroxene + plagioclase + amphibole + magnetite to produce more evolved compositions and associated gabbro cumulates (50% clinopyroxene, 45% plagioclase and 5% titanite; Gruender et al. 2010; Price et al. 2016). During this stage, plagioclase is concentrated in the mobile residual melt and magnetite, often associated with clinopyroxene and amphibole settle (Figure 4). Crustal assimilation throughout this stage is minor. The last fractionation step occurs in the shallow crust, where drier melts evolved to andesitic compositions, and may mix (Figure 4) (Price et al. 1999; 2016). In more hydrous melts, fractionation of amphibole (and biotite) drives compositions towards the dacite field and generates higher incompatible element and K-contents.

Compared to the contemporaneous central North Island Mt. Ruapehu andesites (Figure 3), the K_2O, and LILE concentrations, and some high field strength elements (HFSE) are enriched within the Mt. Taranaki lavas (Figure 3). Chondrite-normalised light rare earth elements (LREEs) are enriched relative to the heavy-REEs (Figure 3). The most primitive Mt. Taranaki basalt (in Price et al. 1992), shows similar high K_2O, Al_2O_3, Rb, Ba and Ni concentrations to TVZ dacites (cf., Graham and Hackett 1987). Mantle-normalised trace element abundance patterns for Taranaki lavas are typical of convergent margin magmas (cf., Sun and McDonough 1989; Kelemen et al. 2005), showing enriched Cs, Rb, Ba and Th (LILEs) relative to mid ocean ridge basalt (MORB), along with high LILE/HFSE and LREE/HREE ratios (Price et al. 1992). Chondrite-normalised REE patterns of Taranaki lavas show weak Eu anomalies (Zernack et al. 2012), indicating limited plagioclase fractionation, late plagioclase fractionation, or plagioclase fractionation under conditions of high oxygen fugacity. The isotope ratio $^{87}Sr/^{86}Sr$ ratios become slightly more radiogenic over time (Zernack et al. 2012), but do not correlate with variations in major and trace element composition in the Taranaki suite, nor with the narrow ranges in $^{143}Nd/^{144}Nd$ and $^{207}Pb/^{204}Pb$ ratios (Price et al. 1992).

Collectively, the compositional data of Taranaki lavas are most consistent with conventional subduction-fluid fluxed melting of a depleted mantle wedge. Parental undersaturated basaltic melts were subsequently modified by fractional crystalisation, but only minor crustal assimilation (Price et al. 1999) (Figure 4). LILE abundances in Taranaki basalts and their silica undersaturated character indicate a low degree of partial melting (Price et al. 1992). High Ba/La ratios indicate a significant input of fluids from a dehydrating subducted slab, but the current data cannot completely rule out metasomatism via a gravitational mantle instability (Figure 4).

The isotopic similarity of the Taranaki and TVZ basalts precludes the deepening source model proposed by Kuno (1966) and Dickinson and Hatherton (1967). The most mafic magmas differ from primitive arc magmas (cf., Tatsumi and Eggins 1995), likely because they have interacted with lower crustal amphibolitic underplate and mush, driving higher incompatible elemental contents (Stewart et al. 1996; Price et al. 1999). This process is partly by subsequent fractionation. A systematic increase in the abundance of incompatible trace element concentrations (Rb, Ba, Zr) and K_2O occurs over time through Taranaki rocks (Price et al. 1999; Zernack et al. 2012) (Figure 3). The $^{87}Sr/^{86}Sr$ isotope ratios are at their highest levels within the youngest samples, but with only a weak systematic relationship seen for older ones. Oxygen isotopes reveal typical values for island arcs, with little evidence for continental crust interaction. Collectively, this information indicates that the magmatic system evolved over time, as temperature gradients increased, along with underplating of the crust, leading to greater interaction with underplated amphibole-rich material. Xenolith suites (Gruender et al. 2010; Price et al. 2016), show evidence for extensive hydrous metasomatism of the upper mantle and lower crustal cumulates. Zernack et al. (2012) and Price et al. (2016) suggested that ~200 kyr of magmatism has progressively altered the crustal thermal state and composition (Figure 4). Over time, new storage zones were formed various depths, that increase the complexity of magma mixing and assembly in the upper crust (10-6 km depth).

The >0.25 Ma Pouakai-sourced rocks (Price et al. 2021), overlap in composition with early Mt. Taranaki lavas, but have lower K, P, Ba, Rb, Sr and Zr and higher Sc and V concentrations than the younger volcano. The compositional variation reflects different degrees of bulk fractionation, with net removal of amphibole and clinopyroxene and consequent concentration of plagioclase phenocrysts. The Pouakai

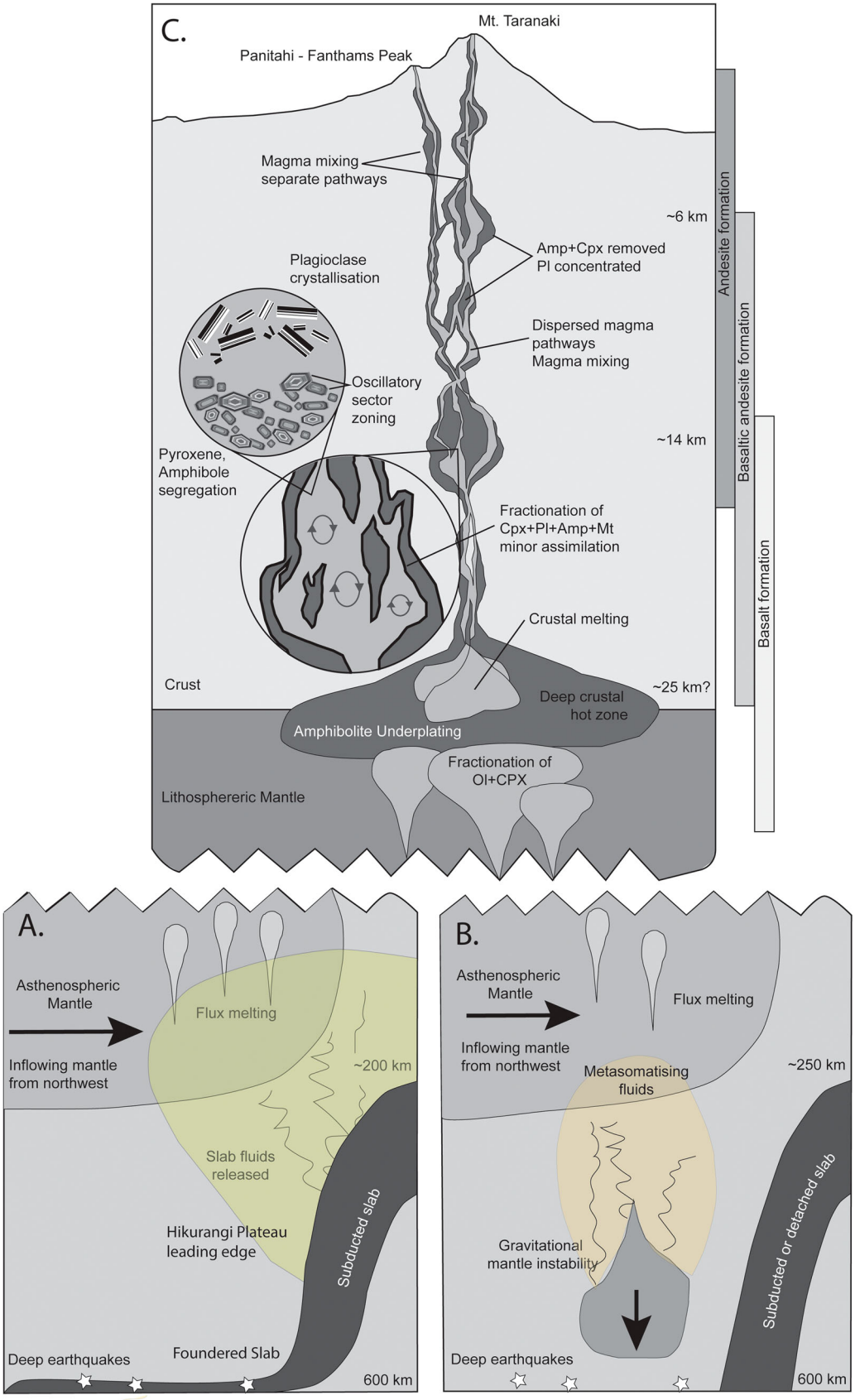

Figure 4. Magma source and processing model for Mt. Taranaki magmas (not to scale). The model outlines the two deep source scenarios from the literature: (A) fluids released from a deep slab flux into a depleted mantle wedge to form small-degree partial melts of undersaturated basalt. The deep earthquakes represent a detached foundered slab. Scenario A is favoured by magma geochemistry (see text); (B) a gravitational instability and lithospheric mantle foundering, with the front generating deep earthquakes seen by Boddington et al. (2004). Fluids released from this body metasomatises mantle material drawn in from the northwest. In the upper system (C) Basaltic magmas evolve and rise by fractionation to accumulate at the base of the crust, gradually forming an underplate of amphibolite, pyroxenite and gabbro. Assimilation of magmas within this zone produces more evolved basalts that rise, further differentiate and mix on polybaric pathways to eruption.

system developed and modified the crust in much the same way as Taranaki volcano (Figure 4).

Taranaki ring plain and volcanic debris avalanches

The overlapping volcaniclastic deposit fans that radially surround Mt. Taranaki are collectively termed a *ring plain* that forms much of the Taranaki Peninsula, comprising a volume of ~150 km^3 and covering an area of >2000 km^2 (Neall 1979; Alloway et al. 1995; Zernack et al. 2011) (Figure 5). These deposits are exposed in coastal cliffs, but debris avalanche deposits extend out to >6–8 km offshore in places (Alloway et al. 2005; Zernack et al. 2011). The main landscape-forming units are debris avalanche deposits formed by major collapses of the volcano flanks (Ui et al. 1986; Palmer et al. 1991; Procter et al. 2009; Zernack et al. 2009; Roverarto et al. 2014; Zernack 2020). The edifice collapses form wide fans over the low-relief paleo-landscape (Procter et al. 2009; Zernack et al. 2009). One or more axes of deposition are marked by frequent 5–50 m-high mounds forming an irregular landscape (Palmer et al. 1991; Palmer and Neall 1991; Procter et al. 2009; 2020). Proximal deposits are highly chaotic diamictons and contain 10–100 m-long mega-clasts and lithologically-uniform domains that represent blocks of semi-intact portions of the cone (Figure 2) (Ui et al. 1986; Roverarto et al. 2014). In distal and lateral margins, the deposits show a uniform matrix dominated by a poorly sorted mix of clay and sand, with heterolithologic clasts, including in-situ fractured clasts and isolated large mega-clasts that are found >45 km from source (Alloway et al. 2005; Zernack et al. 2009). The clay content of the matrix is typically 10–15 wt%. Breakage of slide blocks and comminution of softer, pumice and weathered clasts during flow generated the matrix phase (Roverarto et al. 2014).

Each discrete debris avalanche blanketed between 100 and >350 km^2 with 5–50 m of material (Zernack et al. 2011) (Figure 5). Intercalated between debris avalanche units are lahar deposits (debris flow and hyperconcentrated flow units; Zernack et al. 2009), and nearer to the cone, pyroclastic flow deposits (Lerner et al. 2019b; Lerner et al. 2019c). Using a series of interglacial marine-cut terraces, peats and tephras, a stratigraphy of 16 debris avalanche events is constructed (Alloway et al. 2005; Zernack et al. 2011) (Figure 5).

Mt. Taranaki sourced deposits wrap around an older 360 km^2 ring plain sourced mainly from Pouakai volcano (Gaylord and Neall 2012; Gaylord et al. 2014). The Pouakai ring plain sequence is capped by a >7.5 km^3, 240–210 ka debris avalanche deposit. This event is attributed to the volcanic pile spreading on weak, saturated and shallow-dipping Pliocene marine mudstones (Gaylord and Neall 2012). This mechanism contrasts with internal-edifice failures associated with Mt. Taranaki (Zernack et al. 2009; 2012).

The oldest recognised Mt. Taranaki debris avalanche deposits outcrop along on the northern coastline between western New Plymouth to Onaero (Figures 1 and 5). The Mangati Formation (Zernack et al. 2011), overlies the Ngarino marine bench, formed at ~210 ka (Pillans 1983; 1990). It is covered by peat with interbedded tephra, and the Motunui debris avalanche deposit (Alloway et al. 2005). The Motunui unit is cut by the tread of the Rapanui marine terrace (~127 ka; Pillans 1983; 1990). The youngest north-distributed Okawa debris avalanche deposit is mapped between Inglewood to a broad fan centred around Waitara (Alloway et al. 2005) (Figure 5). Using pollen records Alloway et al. (2005) estimated its age at ~105 ka.

A group of debris avalanche deposits aged between ~90 and 60 ka, are exposed along the south (Oeo) and southeastern coast (Waingongoro, Waihi, Tokaora) as well as within boreholes to the east of Mt. Taranaki (Figure 5). The Oeo unit (~90 ka) overlies the Inaha Marine bench (~105 ka; Pillans 1983; 1990), and is capped by a buried forest and peat of ~80 kyr old (Zernack et al. 2011). Waingongoro and the overlying Waihi units are separated only by a thin paleosol, but separated from the lower Oio unit by a thick stack of weathered tephra, sand and peat. The ages of the two units are stratigraphic estimates of 75 ka (Waingongoro) and 70 ka (Waihi) (Zernack et al. 2011). Above pumice-rich hyperconcentrated flows, fluvial sands and pebble beds, the Tokaora debris avalanche unit is estimated at ~60 ka (Zernack et al. 2011).

The ~55-30 ka debris avalanche deposits are exposed along the southern coast. Otakeo, Kaupokonui and Rama units, are interbedded by hyperconcentrated flow and peat units. Peat above the Rama unit is dated at ~36 ka BP (Zernack et al. 2011). Two younger units farther south east include the Ihaia unit that includes 37 ka BP dated wood, and the Te Namu unit, containing wood spanning 34–37 ka BP in age (Zernack et al. 2011).

Two closely timed debris avalanche deposits produce a mirrored deposition pattern over vast areas east (Ngaere Formation) and west (Pungarehu Formation) of the volcano (Figure 5). Fall deposits of the 25 ka BP >500 km^3 rhyolitic Oruanui caldera-forming eruption of Taupo Volcano overlie the ~27 ka Ngaere but closely underlies the ~25 ka Pungarehu debris avalanche unit (Alloway et al. 2005; Zernack et al. 2011). Following these events, the two youngest debris avalanche deposits are exposed to the south west, including the Motumate (14 ka BP) and the Opua (7.5 ka BP).

Of the 16 debris avalanches known from Mt. Taranaki, three have minimum estimated volumes of

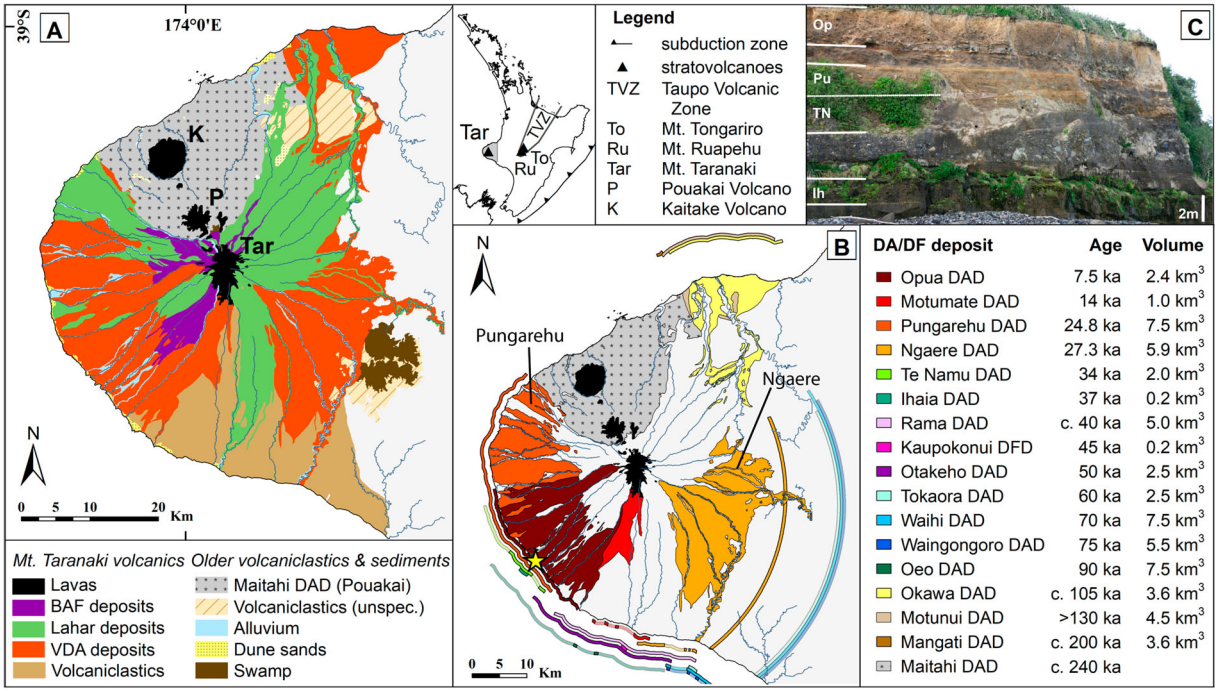

Figure 5. The Taranaki ring plain. **A**. Volcanic geological map of the Taranaki Peninsula showing the main landscape-forming volcaniclastic units and three Taranaki Volcanic Lineament edifices (K = Kaitake, P = Pouakai, Tar = Taranaki Volcano). **B**. Map, ages, volumes and distribution pattern of the 16 debris avalanche deposits (Alloway et al. 2005; Zernack et al. 2011). The colour bands around the coast show the relative stratigraphy and outcrop patterns for buried overlapping debris avalanche deposits exposed in coastal cliffs. **C.** A typical coastal exposure at the location marked with a yellow star in frame B. Opua (Op), Pungarehu (Pu), Te Namu (TN) and Ihaia (Ih) are deposited here, with interbedded fluvial sands, gravels and conglomerates.

7.5 km^3 (Oeo, Waihi, and Pungarehu), six others are between 3.5 and 6 km^3 (Mangati, Motunui, Okawa, Waingongoro, Rama and Ngaere), three ~2.5 km^3 (Tokaora, Otakeho, Opua), and three are <1 km^3 (Kaupokonui, Ihaia, Motumate). The flows ran out at least 25–46 km from source (Alloway et al. 2005; Zernack et al. 2011). The largest deposits are equivalent to at least 60% of the present volume of the Mt. Taranaki edifice above ~1400 m-elevation. The unit distributions imply that collapses occurred from all directions of the edifice (except the buttressed northwest).

Mt Taranaki shows strong pre-conditioning factors for volcanic slope failure, including: steep slopes, weak pyroclastic deposits, very high rainfall rates, buried faults and a weak sedimentary substrate. Currently, evidence of triggering mechanisms for flank collapse are elusive. There is generally a low proportion of hydrothermally altered clasts, indicating a lack of pervasive hydrothermal weakening of past edifices. Alloway et al. (2005) attributes one event, the Ngaere, to intrusion of new magma based on a widespread 'blast-deposit' tephra immediately below it (a Bezymianny-type collapse; Siebert et al. 1987). The southern-distributed debris avalanches are rich in pumice, and thus could also have been caused by intrusions. Additional triggering mechanisms are suggested by a series of at least 13 major earthquakes ($M_{6.1}$ to $M_{6.6}$) along faults near, or below the edifice over the last 26 kyr (Townsend et al. 2010). Some of these events generated ground motions of up to 1.5 m and fault-length ruptures of 25–30 km. These could trigger 'Unzen-style' (Siebert et al. 1987) flank collapses and debris avalanches without associated volcanic activity. Debris avalanche distributions are consistent with a N-S orientation of faulting and dyke expansion beneath Mt. Taranaki. The collective ~13.5 km^3 collapsed in the closely spaced Ngaere/Pungarehu events suggests that the edifice was very large at the time and the first collapse may have destabilised it to generate the second.

The role of glaciers and ice/snow loading is difficult to evaluate, since most of the upper slopes are post-Glacial in age. Thick lava buttresses between 1400 and 1000 m around the volcano are similar to ice-bounded lavas seen on other stratovolcanoes such as Mt. Tongariro and Ruapehu, but Zernack et al. (2012) found little temporal relationship between Mt. Taranaki collapse timing and the major Last Glacial and Interglacial events.

Immediately following debris avalanches, multiple smaller landslides and lahars occurred as landscapes rapidly re-adjusted (Procter et al. 2009). The lithology of lahar deposits show that stratovolcano regrowth involved periods Plinian eruptions (mainly pumice-rich deposits), or dome-growth episodes (mainly dense lava-clasts) (Zernack et al. 2009). Within ~15 km of the summit, deposits are younger and

dominated by mainly dome-collapse pyroclastic flow units (Block-and-Ash Flow deposits/BAFs) and associated lahars, such as the ~8–12 ka BP Kahui Formation (Neall 1979; Alloway et al. 1995), and the <1 ka BP Maero Formation (Neall 1979; Platz et al. 2012; Lerner et al. 2019b; Lerner et al. 2019c).

Taranaki tephrochronology and cyclic eruption rate

Fall deposits spanning the last ~30 ka BP of pyroclastic activity from Mt. Taranaki are preserved mainly east of the volcano, dispersed by the prevailing westerly winds (Neall 1972; Alloway et al. 1995). With increasing age, highly weathered tephras are indistinct and intercalated with volcanic loess deposits on the oldest landscapes (Alloway et al. 1992). Within post ~30 ka soils, a stratigraphy of 76 tephras is mapped within 16 named tephra formations (Alloway et al. 1995). The chemical and petrological similarity of these tephras, however, hinders ready correlation and identification of individual units (Cronin et al. 1996; Platz et al. 2007b). Soil sequences record mainly the largest and coarsest tephras, estimated with volumes of >0.1 km^3 (Alloway et al. 1995). Taranaki tephras are very widespread, with one unit per 1.4 kyr found in >80 ka-long lake and peat records within maar lakes in Auckland, 270 km to the north (Molloy et al. 2009).

A higher resolution tephra sequence is found within radiocarbon-dated swamp and lake sediment sequences around the volcano (Figure 1) (Turner et al. 2008c; 2009; Damaschke et al. 2017a; Damaschke et al. 2017b). This helped identify regional correlation errors in earlier soil-based stratigraphy (Damaschke et al. 2017b) (Table 2), as well as highlighting an underestimate of eruption rates. The tephras range from >30 cm-thick med-lapilli pumice units down to 0.5 mm-thick medium ash. Lake Umutekai, north of Mt Taranaki, revealed 123 eruptions over the last 10 ka BP, and significant time-variability was noted in the tephra fall rate (Turner et al. 2008c). Adding the Lake Rotokare record, southeast of the volcano, and accounting for correlatives using geochemistry and age-overlaps, Turner et al. (2009), identified a more-complete record of 138 eruptions over the same period. Subsequently, with six lake and swamp sites spanning a 120-degree downwind arc, and using 50 new radiocarbon dates, Damaschke et al. (2017a; Damaschke et al. 2017b) identified 228 tephra-producing eruptions over the last 30 ka BP. Even in this very high-resolution record, some time periods are covered by only one site, and there is a major depositional gap in the sequences during the last Glacial maximum (~23.5–17.5 ka BP) (Damaschke et al. 2018). Thus, the true explosive eruption history remains underestimated. The increasing resolution provided by successive studies has preserved a strong time variability of Mt. Taranaki eruption rates, showing it is a real feature of the volcanic system and not a preservation bias (Figure 6A).

Some time-variability in eruption rates may relate to eruption style variations; i.e. small dome collapse events (Platz et al. 2007), vs. larger Plinian/sub-Plinian events (Torres-Orozco et al. 2018). In dome-collapse events, tephra deposition is localised (Druce 1966; Platz et al. 2007; 2012). To overcome this, Turner et al. (2008b) distinguished dome-forming events from sub-Plinian/Plinian eruptions using exsolution textures in titanomagnetite grains. Slow-rising magmas in conduits feeding domes show distinct exsolution within the ulvöspinel. By contrast, rapidly rising magmas feeding Plinian-style eruptions are chilled rapidly with little or no exsolution observed (Turner et al. 2008b). With dome-related tephras removed from the sequence, there is a strong regular variability in the sub-Plinian/Plinian eruption rate. Over a period of ~1500 years, Plinian-style eruptions varied in rate between ~5 and ~14 events/kyr (Turner et al. 2008b). This broadly relates to changes in tephra composition; with more mafic compositions associated with the higher eruption-rates (Turner et al. 2011b). The most silicic and largest volume tephras occur mainly during periods of low eruption rate. Turner et al. (2011b) identified that periodic recharge of new magma to mid-crustal reservoirs could explain this variability and identified six compositionally distinct 'batches' of magma entering the system over the last 12 ka BP.

Chemically (and physically) identifying individual tephras remains difficult, so that tephra sequences are mainly correlated as compositional groups. Damaschke et al. (2017a; Damaschke et al. 2017b) used electron-microprobe determined glass (mainly SiO_2, CaO and FeO) and titanomagnetite chemistry (mainly MgO, Al_2O_3, TiO_2, and Fe^{3+}) to separate the post-18 ka B.P. tephras into 12 titanomagnetite compositional groups, expanding on the magma batches defined by Turner et al. (2011a). However, Damaschke et al. (2017a; Damaschke et al. 2017b) recognised that the compositional groups do not define a simple unique temporal sequence; instead compositions repeat over time and more than one batch may erupt contemporaneously. Despite this, the compositional batches define six sequential tephra sequences within a robust chemical chronostratigraphy (Table 1). Most tephras have trachyandesite to trachydacitic glass compositions (<67% wt% SiO_2), but the thickest and coarsest units are generally more evolved (~69–74% wt% SiO_2 in glass). The highest silica glass is associated with titanomagnetite grains with lowest Al_2O_3, MgO and TiO_2 and highest FeO_{tot} concentrations. Some of the tephra sequences show narrow ranges in glass and titanomagnetite compositions

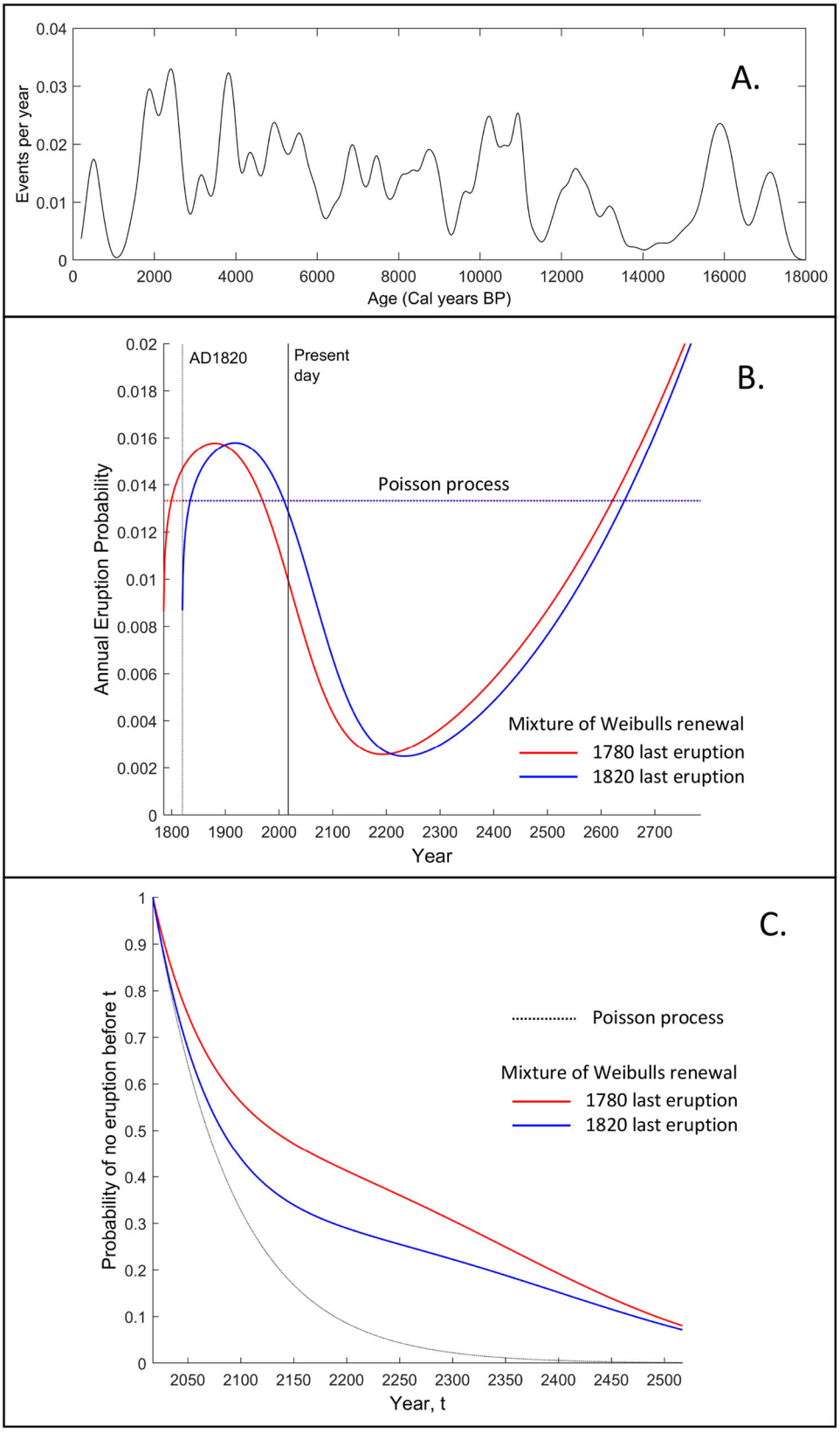

Figure 6. Eruption frequency of Mt. Taranaki and probabilistic eruption forecasts. A. A frequency curve showing the most recent collective record of tephra eruptions of all types from medial lake and swamp sequences in the eastern Taranaki region (Damaschke et al. 2018). Note the regular variation in eruption frequency. B. Current annual probabilistic forecast for the next eruption based on the most recent age data, modelled from the distribution of inter-event times over the last 10 ka B.P. The Poisson process assumes random eruption recurrence (flat line). The mixture of Weibulls model is preferred because it accounts for two distributions of inter-event times seen in the Taranaki data, including short (~65 years) and long (~580 years) modes. The decrease in the eruption probability indicated by the Weibulls model by 2200 reflects transition from the short-interval distribution to that of long-intervals. The red and blue Weibulls curves represent the extremes in age uncertainties of the last eruption (1780 to 1820). C. Forecast of cumulative probability of eruption from Mt. Taranaki using the same models as for B. The Poisson process indicates a more rapid progression to eruption after 100 years of quiescence than the mixture of Weibulls models based on the extremes of age estimates.

Table 1. Chemically defined chronostratigraphy of tephras based on titanomagnetite chemical groupings (Tm-group), erupted from Mt. Taranaki over the last 30 ka BP from Damaschke et al. (2017a, 2017b). Named correlatives can be chemically matched to cores (although note that the original definitions group several units under the same name). Named units in brackets are correlated by age, but cannot be identified by their chemistry.

Tephra Seq.	Age cal ka BP	No of tephras	Tm- group	Glass SiO_2 wt%	Distal correlatives	Named tephra correlatives[1]
F	30-23.5	39	1 > 2, 6, 8	58–71	Eg28.9[2]	Poto (Tuikonga, Koro, Pukeiti, Waitepuka)
E	17.5-14.0	35	1	55–63	AT203, T19, At206[3] Eg13, Eg14[4]	(Kaihouri, Paetahi)
D	14.0-9.5	37	2 > 3, 1, 4, 5, 7	60–71	Eg9[4] T7, AT191, AT193[3] Eg12.3, Eg11.7[2]	Kaponga, Konini, Mahoe
C	9.5-4.0	60	8 > 3, 11, 7, 9	66–74	Eg4–7[4]	Tariki, Kokowai, (Mangatoki, Waipuku, Kapuni-A)
B	4.0-3.0	17	10	69–73		Kapuni-B, Upper-Inglewood, Lower-Inglewood (Korito)
A	3.0-0.5	32	11 > 12, 2, 6, 9	52–69		Curtis Ridge[5] Maketawa Manganui-MA to MG

[1]Alloway et al. 1995, p. [2]Shane (2005), [3]Sandiford et al. (2001), [4]Lowe (1988), [5]Turner et al. (2008a)

(e.g. E, B; Table 1), whereas most span a wider range of erupted compositions including some units with high-silica compositions (e.g. during B and C), and others more mafic compositions (e.g. during A). Closely spaced tephra eruptions during sequences C and A, show titanomagnetites and glass falling into widely different populations that indicate co-existing but different pre-eruptive storage and eruption conditions (Damaschke et al. 2017a). This may reflect the complex polybaric models of magma formation suggested for Mt. Taranaki (Price et al. 1999; Turner et al. 2011b; Zernack et al. 2012), and, the possible presence of past parasitic cones like the present Panitahi (Fanthams Peak). The first appearance of tephras with distinct mafic compositions (52–59 wt% SiO_2 in glass, plus high Al_2O_3 + MgO concentrations in titanomagnetite) at ~2.8 ka B.P. is the first definitive evidence of Panitahi (Fanthams Peak) eruptions (Turner et al. 2011b; Damaschke et al. 2017a; Damaschke et al. 2017b).

The variation in frequency of eruptions over time at Mt. Taranaki over the last 18 ka BP (Figure 6A) is more irregular than earlier thought at 1000–1500 yrs, with the lowest frequency periods experiencing ~5–10 events/kyr, but regular high peaks reaching 25–30 events/kyr (Damaschke et al. 2018). Whether all of these variations are represented by recharge remains unclear with present chemical data resolution. Several additional factors may influence eruption rate variability, such as subtle changes in the crustal stress regime, earthquake events, and the regular flank collapses that occur at Mt. Taranaki.

The volumes of tephras have been estimated in two ways. For a small number of units where proximal-medial deposits are well mapped, volumes from modelled isopachs are estimated (Platz et al. 2007; Torres-Orozco et al. 2017). However most tephras, are found only within lake and swamp cores, so statistical approaches were applied (Green et al. 2016). Statistically estimated volumes from partial isopachs presented by Alloway et al. (1995) show that the largest unit Konini.b erupted 0.26 km^3, of tephra, while others are ~0.2 km^3 (Inglewood.b, Paetahi.a, Tuikonga.d), or >0.1 km^3 (Manganui.b, Korito.b, Tariki.e, Kaponga.f, Koru.a). Green et al. (2016) modelled volumes based on comparative tephra thicknesses within local lake and swamp cores, as well as correlated tephras in distal cores in Auckland (270 km north) and near Ruapehu (~140 km east). This showed that the 228 tephras range between 0.2 and 0.07 km^3 (Green et al. 2016). There are major errors involved in these estimates, because many tephras are represented at only one or two sites, and thickness variations within sites are common. Despite this, Green et al. (2016) noted a weak correlation of increasing repose periods with the highest volume eruptions. Using newly collected field isopach data for <5 ka BP units, Torres-Orozco et al. (2017), showed that the largest tephras were likely greater in volume, including Kokowai at 0.3–0.5 km^3, Manganui 0.35–0.41 km^3, Inglewood 0.22–0.24 km^3, and Burrell and Kaupokonui at 0.08–0.1 km^3. For the largest <5 ka BP eruptions, Kokowai and Inglewood, Torres-Orozco et al. (2017) estimated eruption column heights at ~28 km, under typical windspeeds of 20–30 m/s. The Manganui heights were ~24 km and the others were all consistent with sub-Plinian events at ~14 km-high. Calculated mass eruption rates were 10^7–10^8 for Kokowai, Inglewood and Manganui, consistent with Plinian eruptions, while the others are in the sub-Plinian range (cf., Bonadonna and Costa 2013).

Proximal flank pyroclastic sequences and eruption scenarios

The most detailed insights into the range of volcanic processes on Mt. Taranaki over the last ~8 ka BP come from proximal exposures on the volcano flanks

above 1200 m (Druce 1966; Neall 1979; Platz et al. 2007; 2012; Turner et al. 2008a; 2011a; Torres-Orozco et al. 2017). Linking cone-construction to tephra records is challenging, because lava ages are constrained only by few paleomagnetic studies (Downey et al. 1994; Lerner et al. 2019a). By chemically correlating pyroclastic deposits intercalated with lava flows on the flanks with well-dated lake-core tephra records, Turner et al. (2011a) showed how much of the upper cone was built by lava flow effusion between 6 and 5 ka BP. This fits with cone re-growth following the >2.4 km^3 Opua Debris avalanche (7.5 ka BP; Zernack et al. 2011). Panitahi cone and associated lavas were emplaced post ~3.3 ka BP (Turner et al. 2011a Torres-Orozco et al. 2018), while the latest episodes of the summit cone lava flows were emplaced between 1300 and 400 yrs ago (Downey et al. 1994), contemporaneously with a highly active period of dome effusion (Lerner et al. 2019b).

The eastern volcano flanks preserve 53 geologically distinct eruptive episodes over the last ~5 ka BP (Torres-Orozco et al. 2017), nine fewer than within equivalent lake/swamp records. The proximal sequences, however, preserve detailed evidence of separate eruptive phases and coeval processes during eruption episodes (Figure 2) (Torres-Orozco et al. 2018). On the north-west flanks, Lerner et al. (2019b) quantify the locus of flank pyroclastic activity since AD 960, including 11 distinct eruptive episodes (the Maero Eruptive Period), that match 6–8 tephras in lake/swamp records. In all cases on the flanks, deposits of eruption episodes are separated by soils and other evidence of dormancy for decades or more. Each episode may include deposits representing different events that span days to weeks to years. The flank deposits include spatially dispersed or overlapping coeval and sequential events during eruption episodes, such as: domes, lava flows, falls, Ballistics, dome-collapse block-and-ash flows (BAFs), column-collapse pyroclastic density currents, blasts, surges, and associated lahars (Figure 2) (Torres-Orozco et al. 2018).

Almost all known eruption episodes at Mt. Taranaki include some form of pyroclastic density current. Most of these are related to the formation and collapse of domes to produce BAFs. These range from marginal gravitational collapse of growing or cooling domes (Platz et al. 2012; Turner et al. 2018; Lerner et al. 2019a); large-scale collapses of freshly emplaced hot domes (Lerner et al. 2019b; 2019d); and deep-seated collapses of domes or crater-rims generating blasts from gas-rich dome-interiors (Druce 1966; Lerner et al. 2019b). In all cases the summit crater was the locus of this activity, and BAFs ran out 5 to >13 km from source (Platz et al. 2007; Procter et al. 2010). Typical BAF volumes are $2–4 \times 10^7$ m^3 and are associated with minor tephra falls and low-particle density surge deposits (Torres-Orozco et al. 2017; Lerner et al. 2019b).

Sub-Plinian or Plinian activity also generated column-collapse pyroclastic density currents (PDCs) (Platz et al. 2007b; Torres-Orozco et al. 2017; 2017; 2018; Lerner et al. 2019c). These deposits reflect unsteady and collapsing eruption columns, and consist of pumice with a wide range of density, along with dense, juvenile lithic clasts (Platz et al. 2007; Torres-Orozco et al. 2017; Torres-Orozco et al. 2017). Typical column-collapse PDCs for sub-Plinian eruptions have volumes and runouts similar to BAFs. However, a few larger column-collapse PDCs, associated with the largest Plinian eruptions, have volumes of $>6 \times 10^7$ m^3, and run out to between 19 and 25 km from source (Torres-Orozco et al. 2017; Lerner et al. 2019c).

All BAF and column-collapse PDC deposits show thermo-remanent magnetisation evidence for pyroclasts travelling at high temperature, with most emplaced at temperatures above the Curie-point (>500°C) (Lerner et al. 2019d). Some flows show signs of cooling with travel distance, and were emplaced at intermediate temperatures between 400 and 200°C (Turner et al. 2018; Lerner et al. 2019d). The largest known column collapse PDC shows temperatures of matrix and clasts at ~23 km from source of between ~300 and >580°C (Lerner et al. 2019c). Sub-Plinian to Plinian eruptions from Panitahi have more uniform pumice textures, and likely had steadier eruption columns producing few and small associated column-collapse PDCs (Torres-Orozco et al. 2017; 2018). The later phases of some Panitahi eruptions included spatter-fed lava flows (Torres-Orozco et al. 2018).

The patterns identified in complex pyroclastic depositional facies in the ~ 53 eruption episodes of the last ~5 ka BP at Mt. Taranaki led Torres-Orozco et al. (2018) to classify three main sub-Plinian and Plinian eruption scenarios. These include: summit dome collapse and conduit-decompression; transient summit conduit clogging and explosive release: and Panitahi open-vent eruptions. These episodes include as many as ten separate eruptive phases, with one or more climactic fall-producing events, along with dome-growth/collapse and associated blasts. The most complex sequences occurred at the summit vent. An event-tree approach by Torres-Orozco et al. (2018) highlights a wide diversity of eruption outcomes, reflecting vent site, conduit/vent state, and gas-coupling with the magma. Some of the intra-episode variability can be directly related to the range in pyroclast textures and magma compositions. The complex summit eruptives are more silicic, and also typically showed large within-episode chemical variation, for example the AD1655 Burrell Lapilli (whole-rock SiO_2 55–60 wt%, MgO 2.5–3.6 wt%, K_2O 2.2–3.3 wt% Torres-Orozco et al. 2017). The

more mafic compositions (whole-rock SiO_2 48–51 wt %, MgO 4–7 wt%, K_2O 1.2–1.9 wt% Torres-Orozco et al. 2017) erupted at Panitahi led to simpler open-vent conditions, with rapid escalation to climactic-height plumes and rapid decay to fire-fountaining (Torres-Orozco et al. 2018).

Pumice erupted during each Plinian episode typically plots within its own array, e.g. on a SiO_2 vs. K_2O plot, so they likely represent separate magma batches (Torres-Orozco et al. 2017). Many of these variations can be attributed to eruptive sequences tapping progressively deeper zones within a density or viscosity segregated conduit or shallow reservoir with segregated crystal-poor magma vs. crystal-rich mixtures (Torres-Orozco et al. 2018).

Patterns in changing or uniform eruption styles over time are observed at Mt. Taranaki (Turner et al. 2008a, 2011a). Lerner et al. (2019b) described a series of events from AD960 to AD1790 with a similar, narrow range of compositions as the Maero Eruptive Period. Two sub-Plinian eruptions occurred during the 11 episodes of this period, but the chemical and physical diversity between eruptions was less than observed for the wider record of the volcano. If the volcano remains within this activity 'regime', then there is possibly a tighter range for the possible future hazards and a more limited number of scenarios possible (Lerner et al. 2019b). However, the relatively long dormancy since the last eruption may indicate that the recharge and intrusion events that drove the Maero Eruption Period are over and new activity could take a different form.

Recognising that the current summit crater is breached to the west and the active crater is currently covered by at least half of an unstable lava dome (Platz et al. 2012; Zorn et al. 2018; Lerner et al. 2019a), future eruptions must begin with intrusion and collapse of the summit dome or breaches beneath this. By contrast, an eruption vent through the scoria cones on Panitahi is more readily excavated by rising magma and gas. Along with onset flank-collapse or debris avalanches of diverse scales and deposition areas, five eruption scenarios are expected from future eruptions of Mt. Taranaki (Figure 7), including:

(a) Burrell-Type. A Magnitude 4–4.5 (calculated after Pyle 2000) (volume 0.1–0.2 km^3), summit eruption that may last weeks to a month or more (e.g. AD1655 AD Burrell eruption; Platz et al., 2007; Torres-Orozco et al. 2018; and Lerner et al. 2019b). It begins with rapid dome effusion and collapses producing hot BAFs that reach 5–13 km from source. Rise of hot, gas-rich magma follows dome unroofing and rapidly produces a sub-Plinian eruption column (15–20 km-high) with downwind lapilli fall out to ~20 km from source and widespread dispersed ash (>250 km). Small partial column-collapses produce pumice-rich PDCs out to ~10 km from source. The later stages include slow effusion of a summit tholoid, along with rainfall remobilisation of pyroclastic deposits into widespread lahars that travel down many of the radial catchments affected by BAF/PDCs as well as tephra fall.

(b) Manganui D-Type. This is a Magnitude 4.9–5.0 (volume 0.3–0.5 km^3) Panitahi vent eruption that may last days to weeks (e.g. 2600 yrs BP Manganui-D eruption; Torres-Orozco et al. 2018). It begins with a rapid vent clearing with Vulcanian explosions followed by violent Strombolian eruptions, which rapidly lead into a climactic sub-Plinian to Plinian scale eruption column (25–27 km) and widespread lapilli fall reaching ~30 km as well as very widespread ash dispersal >250 km downwind. Partial column collapses may occur generating PDCs out to ~5 km from source. As the eruption subsides, it transitions to fire-fountaining and production of minor lava flows. Subsequent rainfall distributes lahars off the flanks affected by tephra fall.

(c) Upper Inglewood Type. This is a Magnitude 4.7–5.5 (volume 0.3–0.6 km^3) long and complex summit eruption (e.g. 3300 yrs BP Upper Inglewood eruption; Torres-Orozco et al. 2018, or ~10 ka BP Konini eruption; Damaschke et al. 2017b; Lerner et al. 2019c). This episode may last several months to years and include several episodes of summit lava dome effusion and collapse, along with repeated explosive dome disruption events. It may include one or more climactic phases with the largest events producing Plinian-scale eruption columns (22–27 km), with lapilli fall reaching 30 km and ash dispersed >250 km. Multiple repeated BAFs, surges and column-collapse PDCs occur, with the largest reaching over 25 km from source. Final eruption phases may include extensive lava effusion with minor ash. Large, widespread lahars are expected to follow due to rainfall remobilisation of pyroclastic deposits surrounding the entire edifice, but especially in catchments with major valley-fills of pyroclastic debris.

(d) Pyramid type. This is a Magnitude 2–3 (volume 0.002–0.03 km^3) effusive summit eruption that may last weeks to many months (e.g. AD1790 Pyramid dome eruption; Platz et al. 2012; Lerner et al. 2019a). The episode involves repeated dome effusion along with several episodes of dome collapse producing BAFs out to 5–10 km from source (Procter et al. 2010). Lava flows may also characterise phases of eruption, during high eruption rate of degassed hot lava. Dome

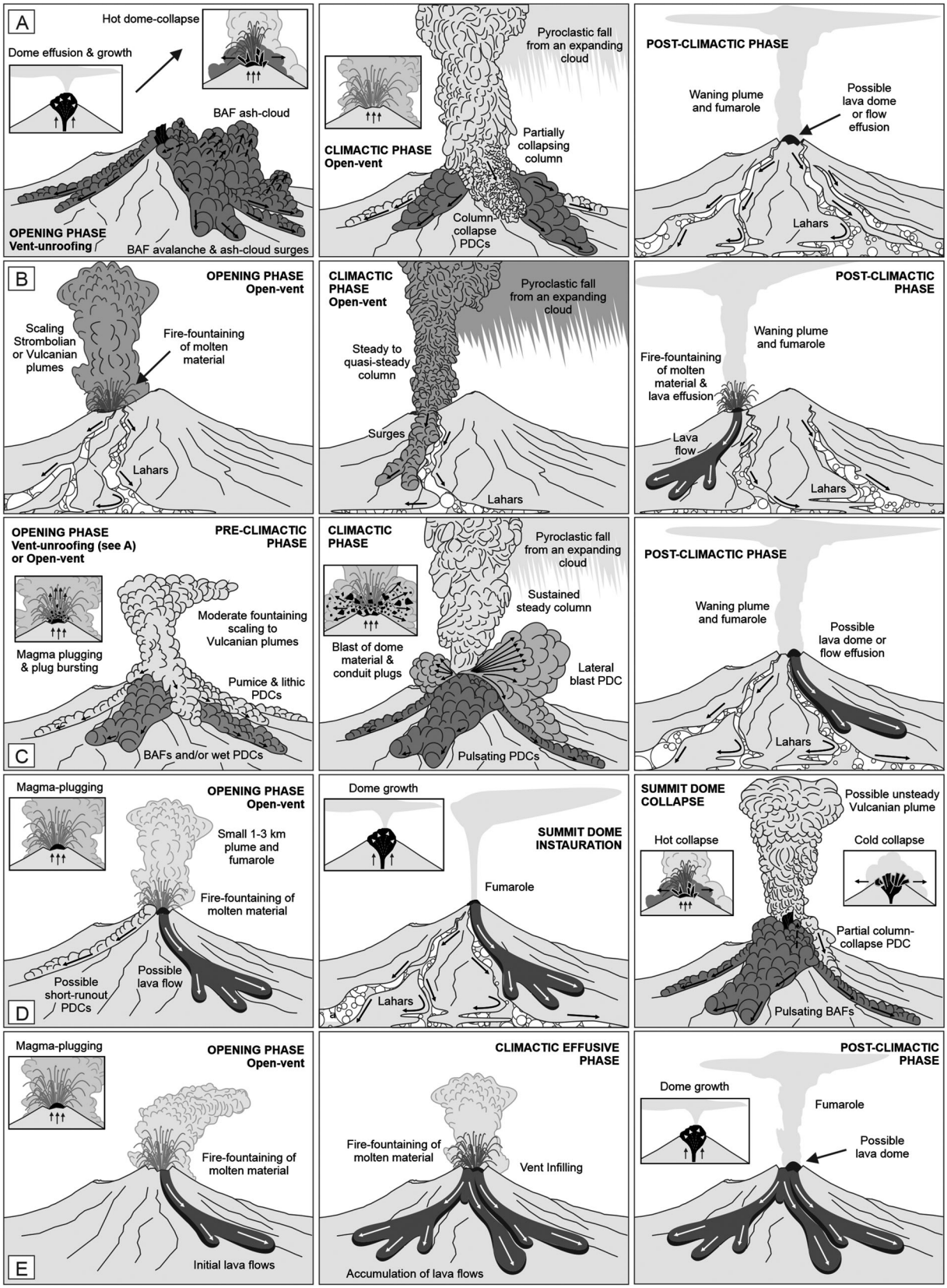

Figure 7. Eruption scenarios expected for Mt. Taranaki based on reconstructed eruption sequences on proximal and medial pyroclastic sequences. **A**. Burrell-Type, a 0.1–0.2 km^3, summit eruption that may last weeks to a month or more (e.g. AD1655 AD Burrell eruption). **B**. Manganui D-Type, a 0.3–0.5 km^3 Panitahi vent eruption that may last days to weeks (e.g. 2600 yrs BP Manganui-D eruption). **C**. Upper Inglewood Type, a 0.3–0.6 km^3 long and complex summit eruption (e.g. 3300 yrs BP Upper Inglewood eruption; or ~10 ka BP Konini eruption). **D**. Pyramid type, a 0.002–0.03 km^3 effusive summit eruption that may last weeks to many months (e.g. AD1790 Pyramid dome eruption). **E**. Staircase type, a 0.02–0.1 km^3 effusive summit (or Panitahi) eruption that may last weeks to months (e.g. the Staircase lava flow sequence).

collapses may unroof degassed portions of domes forming short-lived Vulcanian eruption columns that produce local tephra fall and distal fine-ash out to >30 km from source, along with localised (<5 km) PDCs.

(e) Staircase type. This is a magnitude 3 (volume 0.02–0.1 km^3) effusive summit (or Panitahi) eruption that may last weeks to months (e.g. the Staircase lava flow sequence; Downey et al. 1994). This sequence is associated with small phreatic and vulcanian eruptions that open the vent area, followed by fire-fountaining fed lava flows that escape the low points in the summit crater and follow major valleys to form staked sequences of lavas extending 2–5 km down slope. A tholoid may form over the vent in the final stages.

Probabilistic hazard forecasting

The geological record at Mt. Taranaki has been used for two types of probabilistic hazard assessment. The first of these involved the record of volcanic flank collapses (timing and volume) to forecast the size and timing of the next debris avalanche (Zernack et al. 2012). The chemical composition over the lifespan of the volcano shows a steady evolution in composition, with a generally rising K_2O content. Each debris avalanche deposit appears to represent a separate suite of magmas erupted over this evolutionary pathway (Zernack et al. 2012). Assuming a constant supply of magma and constant basement conditions over the long term, and noting no correlation between the timing of collapse and glacial cycles, the stability of the Mt. Taranaki edifice was assumed to be a function of steady state growth to an unstable size. Thus over time, the chances of collapse rise as the volcano grows, with increasing time intervals associated with larger-volume collapses. Using the past volumes and ages estimates of collapses, an envelope defining the maximum potential size and time between all past collapses was established (Zernack et al. 2012). The calculated average magma extrusion rate over the last 130 ka was estimated at 0.45 km^3/kyr. The edifice stability limit (maximum possible size of a collapse) is estimated from the envelope at ~15.5 km^3 and thus the maximum time between collapses is on the order of 30–35 kyr. Based on the present position in relation to this stability limit, the current maximum size of collapse possible is 7.9 km^3, with a collapse almost certain by 16.2 kyr from now (Zernack et al. 2012). Based on modelling the collapse event history with a Weibull distribution, the current annual probability of a collapse is ~0.02%.

The second probabilistic forecasting work rests on high-precision tephra records (Turner et al. 2008c; 2009; Damaschke et al. 2018; Lerner et al. 2019b). The statistical distribution of the length of dormancy periods between eruptions shows a bimodal distribution, with both short and anomalously long repose periods. The eruption record is simulated using a renewal model that relies on a mixture of Weibull distributions (fitted to each repose-period mode) Turner et al. (2008c). The most recent version of this model contains one distribution with a short mean repose period of 65 years, and a secondary distribution with a mode at 580 years (Damaschke et al. 2018). The renewal assumption means that the estimated likelihood of an eruption varies with time elapsed since the last eruption. Since the last eruption occurred at AD1790, the volcano is still in the short repose distribution. However, the current interval is long and increasing, hence the chances of this interval being in the long repose distribution is increasing over time. This means that the current estimated annual eruption probability is between 1% and 1.3%, and declining (Figure 6B). In the next 50 years, the probability of at least one eruption (Figure 6C) is between 33% and 42% (Damaschke et al. 2018). The annual probability of a Pyramid type (D) scenario (Figure 7) is near the average estimate of 1–1.3%, while that of highest magnitude Inglewood type (C), is ~0.2–0.3%, based on the volume-size distribution known to date.

The long repose periods at Mt. Taranaki may relate to cycles of deep magma recharge, as indicated by geochemical variations through the tephra record (Turner et al. 2011a; Green et al. 2013). The long reposes can thus be used to divide the record into regimes with different eruptive characteristics (Bebbington 2007). Lerner et al. (2019b) described the most recent regime as the Maero Eruptive Period. This regime may still be continuing. Based on the chemical stratigraphy seen at Taranaki, the signal of a new regime beginning would be the eruption of a large volume of relatively highly evolved magma compared to the last millennia, followed by a return to more mafic products in later eruptions.

The current eruption record of Mt. Taranaki likely misses some eruptions. A statistical model to estimate missing records, using an assumption of a complete random (Poisson) process controlling eruption onsets was created by Wang and Bebbington (2012). This showed that the record of Turner et al. (2009), which has been significantly improved on by Damaschke et al. (2018), was at least 86% complete over the last 7000 years. Major gaps in the older record (e.g. 18–32 ka BP) remain.

The consequences of any of these eruptions in the Taranaki region is serious. The region is home to over 110,000 people, as well as the only producing New Zealand oil and gas fields, energy resources, major dairy and meat production, along with fertiliser, manufacturing, electricity generation and distribution (McDonald et al. 2017). Focussing on major

infrastructure settings (electricity grid exit points, natural gas treatment plants and major milk and fertiliser factories) in the Taranaki region, Bebbington et al. (2008), estimated a 0.01–0.5% annual chance of shutdowns due to ash fall. Using dynamic economic models McDonald et al. (2017) estimated the impacts of three eruptive scenarios, equivalent to the Pyramid type (D), the Upper Inglewood type (C), and a debris avalanche equivalent to the most recent Opua event (3.4 km^3). A Pyramid-type eruption, so long as impacts were contained primarily within the National Park boundary, induces minor impacts that are recoverable within a year after eruptions cease. An Upper Inglewood-type eruption would generate a > $200 million impact 1 year after the event, with full recovery of the economy taking 5 years. The debris avalanche scenario induces at least ~$400 million impact within a year and permanent structural change to the Taranaki economy, due to loss of productive land and infrastructure. All of these estimates are contingent on eruptions being brief. The complex long eruption types inferred from the geological record of this volcano would lead to much greater consequences. In addition, economic analysis only considered local Taranaki region impacts. The location of Mt. Taranaki with respect to the prevailing wind direction means that most of the highly populous and economically important regions of Waikato and Auckland will also be directly affected by tephra fall.

Conclusions and topics for future work

Mt. Taranaki superficially represents a typical continental arc stratovolcano. Its position in relation to the current subduction system in New Zealand suggests it should be fed by subducted-slab fluids fluxing low-degree partial melts of the mantle wedge. An alternative model of gravitational mantle instability with lithosphere delamination, along with influx of mantle material from the northwest, is a possible origin of Mt. Taranaki parental magma. However, the lava geochemistry leans more strongly towards a direct slab fluid influence. An obvious future direction of research is to attempt via geochemical and isotopic studies to test the two alternative models.

The increasingly incompatible-element rich andesitic magmas at Mt. Taranaki may reflect a progressive modification of the crust, especially the crust-mantle boundary. Over time, beneath Mt. Taranaki, crustal underplating by successive magmas generates high-K magmas that ascend and pond at various levels in the crust, crystallising clinopyroxene + titanomagnetite + amphibole and plagioclase before erupting a range of evolved compositions. The compositions of individual lavas or pyroclastics are strongly related to the crystal cargo, with glass compositions often being often out of equilibrium with the crystals. Gaps in our understanding of this magma generation model include tight constraints on the depths/pressures and water contents of the magmas in storage regions and the extent of connection or mixing between individual melt batches. It is also important to try to characterise the rates of recharge of this system and whether its character changes (e.g. an active crystal mush vs. crystallised cumulates) depending on magma supply rates. It is further very important to apply a range of petrological experimental approaches to establish a link between the pre-eruption storage depth (and age) of magmas that give rise to the range of eruption types seen at Mt. Taranaki.

There is a clear time-variability in all aspects of this volcano's behaviour, from its regular catastrophic cone collapses generating debris avalanches, through to its strong ~1000–1500 yr cyclic variation in eruption frequency. The collapse cycle requires more investigation. Loss of >7.5 km^3 from the volcanic edifice and potentially a ~1000 m-high stack of rock over the magmatic system should induce changes to the volcano's subsequent behaviour. Unfortunately the age constraints on collapse events is poor. Undertaking further tephra-debris avalanche correlation studies and investigation of ages of collapses will help to tighten the resolution linking the records and provide more examples of pre- and post-collapse variations in eruption composition and frequency. The observed relationship between eruption frequency, composition and eruption size should provide insights into the 'pulse' of a magmatic-volcanic system. However, the magmatic models driving this type of behaviour are poorly known. Linking the magmatic system dynamics to the eruption outcomes will help design new process-driven probabilistic hazard estimates, which could be more widely applicable to similar long-lived andesitic volcanoes elsewhere. Targets for this work are crystal-based studies of tephras and lavas, including *in-situ* crystal isotopic and trace-elemental studies to better understand magmatic development, crystal storage and eruption timescales.

The volcanic-tectonic relationships at Mt. Taranaki are largely underexplored. There appears to be a two-stage migration of volcanism, initially south and then south-southeast along the Taranaki Volcanic lineament over the last ~1.75 Ma. However, the resolution of dates in the older part of the volcanic record is poor. Understanding the age ranges, especially of Pouakai and the older record of the Taranaki volcano will help constrain how rapidly volcanism migrated and may help understand what source mechanism is consistent with the change. In more recent volcano-tectonic relationships, there seems to be coincidence in timing reported between past large earthquake motions both east and west of the volcano and major eruptions. Further investigation focussing on

stress modelling is needed to understand how faulting (hidden beneath the volcanic pile, surrounding it, and far-field relating to the Taupo Rift), affects the volcano. Understanding the stress state could be highly useful to understand conditions of flank collapse (e.g. failure along N-S axes to the east and west seen in the recent geological record), and also identify whether aspects of the patterns seen in eruption rate are tectonically influenced.

The benefits of having one of the most-robust temporal records of volcanism at Mt. Taranaki are unique for New Zealand. Other stratovolcanoes, such as Ruapehu or Tongariro have little chance for equivalent length and resolution records, due to the lack of suitable depocenters in the medial downwind areas. Further refinement of the Taranaki record requires finding new deposition records. Along with this, developing a broader chemical database of tephras, investigating proxies for eruption volume and magnitude and refining models using other isotopic methods is important as a tracer of the rates of magma supply and rise. The eruption record could also be improved by a more concerted effort to link the local tephra record to distal, older sequences in Auckland maar craters. Also, now that improved secular paleomagnetic curves are available for this region, a programme of paleomagnetic investigation of tephra cores and lavas, coupled with geochemical studies will be important to link on-and off-cone records of volcanism and improve current eruption scenarios.

Acknowledgements

We acknowledge the funding support of the MBIE Endeavour Programme 'Transitioning Taranaki to a Volcanic Future' UOAX1913. We thank the two journal reviewers and the Special Volume editor James Scott for the helpful comments that helped to improve this manuscript.

Disclosure statement

No potential conflict of interest was reported by the author(s).

Data availability statement

Data sharing is not applicable to this article as no new data were created or analyzed in this study.

ORCID

Shane J. Cronin http://orcid.org/0000-0001-7499-603X
Anke V. Zernack http://orcid.org/0000-0002-5771-7286
Rafael Torres-Orozco http://orcid.org/0000-0003-2214-9829
Geoffrey A. Lerner http://orcid.org/0000-0002-9853-7601

References

Allis RG, Armstrong PA, Funnell RH. 1995. Implications of a high heat flow anomaly around New Plymouth, North Island, New Zealand. New Zealand Journal of Geology and Geophysics. 38:121–130.

Alloway BV, McComb P, Neall VE, Vucetich C, Gibb J, Sherburn S, Stirling M. 2005. Stratigraphy, age, and correlation of voluminous debris-avalanche events from an ancestral Egmont Volcano: implications for coastal plain construction and regional hazard assessment. Journal of the Royal Society of New Zealand. 35:229–267.

Alloway BV, Neall VE, Vucetich CG. 1995. Late Quaternary (post 28,000 year B.P.) tephrostratigraphy of northeast and central Taranaki, New Zealand. Journal of the Royal Society of New Zealand. 25:385–458.

Alloway BV, Stewart RB, Neall VE, Vucetich CG. 1992. Climate of the Last Glaciation in New Zealand, based on aerosolic quartz influx in an andesitic terrain. Quaternary Research. 38:170–179.

Bebbington MS. 2007. Identifying volcanic regimes using hidden Markov models. Geophysical Journal International. 171:921–942.

Bebbington M, Cronin SJ, Chapman I, Turner MB. 2008. Quantifying volcanic ashfall hazard to electricity infrastructure. Journal of Volcanology and Geothermal Research. 177:1055–1062.

Boddington T, Parkin CJ, Gubbins D. 2004. Isolated deep earthquakes beneath the North Island of New Zealand. Geophysical Journal International. 158:972–982.

Bonadonna C, Costa A. 2013. Plume height, volume, and classification of explosive volcanic eruptions based on the Weibull function. Bulletin of Volcanology. 75(8):1–19.

Briggs RM. 1986. Volcanic rocks of the Waikato region, western North Island, and some petrological and tectonic constraints on their origin. In: Smith IEM, editor. Late Cenozoic Volcanism in New Zealand. Royal Society of New Zealand Bulletin 23; p. 76–91.

Cronin SJ. 2013. Stratovolcanoes. Chapter In: Bobrowsky P, editor. Encyclopaedia of Natural Hazards. Springer. Encyclopaedia of Earth Science Series; p. 941–947.

Cronin SJ, Wallace RC, Neall VE. 1996. Sourcing and identifying andesitic tephras using major oxide titanomagnetite and hornblende chemistry, Egmont volcano and Tongariro Volcanic Centre, New Zealand. Bulletin of Volcanology. 58:33–40.

Damaschke M, Cronin SJ, Bebbington MS. 2018. A volcanic event forecasting model for multiple tephra records, demonstrated on Mt. Taranaki, New Zealand. Bulletin of Volcanology. 80(1):Art No 9.

Damaschke M, Cronin SJ, Holt KA, Bebbington MS, Hogg A. 2017a. A new 30,000-year high-precision eruption history for the andesitic Mt Taranaki, North Island, New Zealand. Quaternary Research. 87(1):1–23.

Damaschke M, Cronin SJ, Torres-Orozco R, Wallace RC. 2017b. Unifying tephrostratigraphic approaches to redefine major Holocene marker tephras, Mt Taranaki, New Zealand. Journal of Volcanology and Geothermal Research. 337:29–43.

Dickinson WR, Hatherton T. 1967. Andesitic volcanism and seismicity around the Pacific. Science. 157:801–803.

Dimech J-L, Stern T, Lamb S. 2017. Mantle earthquakes, crustal structure, and gravitational instability beneath western North Island, New Zealand. Geology. 45:155–158.

Downey WS, Kellett RJ, Smith IEM, Price RC, Stewart RB. 1994. New palaeomagnetic evidence for the recent erup-

tive activity of Mt. Taranaki, New Zealand. Journal of Volcanology and Geothermal Research. 60:15–27.
Druce AP. 1966. Tree-ring dating of recent volcanic ash and lapilli, Mt Egmont. New Zealand Journal of Botany. 4:3–41.
Eberhart-Phillips D, Reyners M, Faccenda M, Naliboff J. 2013. Along-strike variation in subducting plate seismicity and mantle wedge attenuation related to fluid release beneath the North Island, New Zealand. Physics of the Earth and Planetary Interiors. 225:12–27.
Elkins-Tanton LT. 2007. Continental magmatism, volatile recycling, and a heterogeneous mantle caused by lithospheric Rayleigh-Taylor instabilities. Journal of Geophysical Research. 112:B03405.
Elkins-Tanton LT, Grove TL. 2003. Evidence for deep melting of hydrous metasomatized mantle: Pliocene high-potassium magmas from the Sierra Nevadas. Journal of Geophysical Research –Solid Earth. 108:2350.
Funnell R, Chapman D, Allis R, Armstrong P. 1996. Thermal state of the Taranaki Basin, New Zealand. Journal of Geophysical Research. 101(25):197–215.
Gaylord DR, Neall VE. 2012. Subedifice collapse of an andesitic stratovolcano: The Maitahi Formation, Taranaki Peninsula, New Zealand. Geological Society of America Bulletin. 124:181–199.
Gaylord DR, Neall VE, Palmer AS. 2014. The Middle Pleistocene Maitahi Formation, Taranaki, New Zealand: a new formal lithostratigraphic unit. New Zealand Journal of Geology and Geophysics. 57:369–377.
Giba M, Nicol A, Walsh JJ. 2010. Evolution of faulting and volcanism in a back-arc basin and its implications for subduction processes. Tectonics. 29:4.
Gow AJ. 1968. Petrographic and petrochemical studies of Mt Egmont andesites. New Zealand Journal of Geology and Geophysics. 11:166–190.
Graham IJ, Hackett WR. 1987. Petrology of calc-alkaline lavas from Ruapehu Volcano and related vents. Journal of Petrology. 28:531–567.
Green RM, Bebbington MS, Cronin SJ, Jones G. 2013. Geochemical precursors for eruption repose length. Geophysical Journal International. 193:855–873.
Green RM, Bebbington MS, Jones G, Cronin SJ, Turner MB. 2016. Estimation of tephra volumes from sparse and incompletely observed deposit thicknesses. Bulletin of Volcanology. 78:25.
Gruender K, Stewart RB, Foley S. 2010. Xenoliths from the sub-volcanic lithosphere of Mt. Taranaki, New Zealand. Journal of Volcanology and Geothermal Research. 190:192–202.
Holt WE, Stern TA. 1994. Subduction, platform subsidence, and foreland thrust loading: The late Tertiary development of Taranaki Basin. New Zealand Tectonics. 13:1068–1092.
Hull AG. 1994. Past earthquake timing and magnitude along the Inglewood fault, Taranaki, New Zealand. Bulletin of the New Zealand Society for Earthquake Engineering. 27:155–162.
Hull AG. 1996. Earthquake and volcanic hazards in Taranaki: potential threats to oil and gas production and distribution infrastructure. New Zealand Petroleum Conference Proceedings. 1:261–271.
Hunt T, Syms MC. 1975. Sheet 7, Taranaki. Magnetic map of New Zealand, 1:250000, total force anomalies. Wellington: New Zealand Department of Scientific and Industrial Research.
Kelemen PB, Hanghoj K, Greene AR. 2005. One view of the geochemistry of subduction-related magmatic arcs, with an emphasis on primitive andesite and lower crust. In: Rudnick RL, editor. The Crust. Treatise on Geochemistry 3, Holland HD, Turekian, KK (Ed). Oxford: Elsevier-Pergamon; p. 593–659.
King PR, Thrasher GP. 1992. Post-Eocene development of the Taranaki Basin, New Zealand: convergent overprint of a passive margin. American Association of Petroleum Geologists Memoir. 53:93–118.
King PR, Thrasher GP. 1996. Cretaceous-Cenozoic geology and petroleum systems of the Taranaki Basin, New Zealand. Institute of Geological and Nuclear Science Monograph. 13:243, 244p.
Knox GJ. 1982. Taranaki Basin, structural style and tectonic setting. New Zealand Journal of Geology and Geophysics. 25:125–140.
Kroeger KF, Funnell RH, Nicol A, Fohrmann M, Bland KJ, King PR. 2013. 3D crustal-scale heat-flow regimes at a developing active margin (Taranaki Basin, New Zealand). Tectonophysics. 591:175–193.
Kuno H. 1966. Lateral variation of basalt magma type across continental margins and island arcs. Bulletin Volcanologique. 29:195–222.
Leake BE, Woolley AR, Arps CES, Birch WD, Birch WD, et al. 1997. Nomenclature of Amphiboles; Report of the Subcommittee on Amphiboles of the International Mineralogical Association Commission on New Minerals and Mineral Names. Mineral Magazine. 61:295–310.
Lerner G, Cronin SJ, Bebbington MS, Platz T. 2019b. The characteristics of a multi-episode volcanic regime: the post-AD960 Maero Eruptive Period of Mt. Taranaki (New Zealand). Bulletin of Volcanology. 81(11):Art. No. 61.
Lerner GA, Cronin SJ, Turner GM. 2019d. Evaluating emplacement temperature of a 1000-year sequence of mass flows using paleomagnetism of their deposits at Mt. Taranaki, New Zealand. Volcanica. 2(1):11–24.
Lerner GA, Cronin SJ, Turner GM, Piispa EJ. 2019c. Recognizing long-runout pyroclastic flow deposits using paleomagnetism of ash. Geological Society of America Bulletin. 131(11-12):1783–1793.
Lerner G, Cronin SJ, Turner GM, Rowe MC. 2019a. Paleomagnetic determination of the age and properties of the 1780–1800 AD dome effusion/collapse episode of Mt. Taranaki, New Zealand. Bulletin of Volcanology. 81 (3):Art No 15.
Locke CA, Cassidy J. 1997. Egmont Volcano, New Zealand: three-dimensional structure and its implications for evolution. Journal of Volcanology and Geothermal Research. 76:149–161.
Locke CA, Cassidy J, MacDonald A. 1993. Three-dimensional structure of relict stratovolcanoes in Taranaki, New Zealand: evidence from gravity data. Journal of Volcanology and Geothermal Research. 59:121–130.
Locke CA, Cassidy J, MacDonald A. 1994. Constraints on the evolution of the Taranaki volcanoes, New Zealand, based on aeromagnetic data. Bulletin of Volcanology. 56:552–560.
Lowe DJ. 1988. Stratigraphy, age, composition, and correlation of late Quaternary tephras interbedded with organic sediments in Waikato lakes, North Island, New Zealand. New Zealand Journal of Geology and Geophysics. 31(2):125–165.
McDonald GW, Cronin SJ, Kim JH, Smith NJ, Murray CA, Procter JN. 2017. Computable general equilibrium modelling of economic impacts from volcanic event scenarios at regional and national scale, Mt. Taranaki, New Zealand. Bulletin of Volcanology. 79(12):Art. No. 87.
Molloy C, Shane P, Augustinus P. 2009. Eruption recurrence rates in a basaltic volcanic field based on tephra layers in maar sediments: implications for hazards in the Auckland

volcanic field. Geological Society of America Bulletin. 121 (11–12):1666–1677.
Morley CK. 2018. 3-D seismic imaging of the plumbing system of the Kora Volcano, Taranaki Basin, New Zealand: The influence of syn-rift structure on shallow igneous intrusion architecture. Geosphere. 14:2533–2584.
Mortimer N, Tulloch AJ, Ireland TR. 1997. Basement geology of Taranaki and Wanganui Basins, New Zealand. New Zealand Journal of Geology and Geophysics. 40:223–236.
Neall VE. 1971. Volcanic domes and lineations in Egmont National Park. New Zealand Journal of Geology and Geophysics. 14:71–81.
Neall VE. 1972. Tephrochronology and tephrostratigraphy of western Taranaki (N108–109), New Zealand. New Zealand Journal of Geology and Geophysics. 15:507–557.
Neall VE. 1979. Sheets P19, P20, & P21 New Plymouth, Egmont, and Manaia: New Zealand Department of Scientific and Industrial Research.
Neall VE, Stewart RB, Smith IEM. 1986. History and petrology of the Taranaki volcanoes. In: Smith IEM, editor. Late Cenozoic volcanism in New Zealand. Royal Society of New Zealand Bulletin 23; p. 251–263.
Norris RJ, Cooper AF. 2007. A Continental Plate Boundary: Tectonics at South Island, New Zealand. American Geophysical Union Geophysical Monograph Series. 175:157–175.
Palmer BA, Alloway BV, Neall VE. 1991. Volcanic-debris avalanche deposits in New Zealand–lithofacies organisation in unconfined, wet-avalanche flows. In: Fisher RV, Smith GA, editor. Sedimentation in volcanic settings. SEPM Special Publication 45; p. 89–98.
Palmer BA, Neall VE. 1991. Contrasting lithofacies architecture in ring plain deposits related to edifice construction and destruction, the Quaternary Stratford and Opunake Formations, Egmont Volcano, New Zealand. Sedimentary Geology. 74:71–88.
Pillans BJ. 1983. Upper Quaternary marine terrace chronology and deformation South Taranaki, New Zealand. Geology. 11:292–297.
Pillans BJ. 1990. Late Quaternary marine terraces, south Taranaki-Wanganui (NZMS sheet Q22 and part sheets Q20, Q21, R21 and R22) 1:100, 000. New Zealand Geological Survey Miscellaneous Series Map, 18. Wellington: New Zealand Department of Scientific and Industrial Research.
Platz T, Cronin SJ, Cashman KV, Stewart RB, Smith IEM. 2007a. Transitions from effusive to explosive phases in andesite eruptions – a case-study from the AD1655 eruption of Mt. Taranaki, New Zealand. Journal of Volcanology and Geothermal Research. 161:15–34.
Platz T, Cronin SJ, Procter JN, Neall VE, Foley S. 2012. Non-explosive, dome-forming eruptions at Mt. Taranaki, New Zealand. Geomorphology. 136:15–30.
Platz T, Cronin SJ, Smith IE, Turner MB, Stewart RB. 2007b. Improving the reliability of microprobe-based analyses of andesitic glass for tephra correlation. The Holocene. 17:573–583.
Price RC, Cronin SJ, Smith IEM, Ukstins IA, Zernack AV. 2021. Formation of crystal-rich, mixed, intermediate lavas at Pouakai Volcano and the evolution of the Taranaki volcanic lineament, western North Island, New Zealand. Lithos. 380-381:105850.
Price RC, Gamble JA, Smith IEM, Stewart RB, Eggins S, Wright IC. 2005. An integrated model for the temporal evolution of andesites and rhyolites and crustal development in New Zealand's North Island. Journal of Volcanology and Geothermal Research. 140:1–24.
Price RC, McCulloch MT, Smith IEM, Stewart RB. 1992. Pb–Nd–Sr isotopic compositions and trace element characteristics of young volcanic rocks from Egmont Volcano and comparisons with basalts and andesites from the Taupo Volcanic Zone, New Zealand. Geochimica Cosmochimca Acta. 56:941–953.
Price RC, Smith IEM, Stewart RB, Gamble JA, Gruender K, Maas R. 2016. High-K andesite petrogenesis and crustal evolution: Evidence from mafic and ultramafic xenoliths, Egmont Volcano (Mt. Taranaki) and comparisons with Ruapehu Volcano, North Island, New Zealand. Geochimica et Cosmochimica Acta. 185:328–357.
Price RC, Stewart RB, Woodhead JD, Smith IEM. 1999. Petrogenesis of high-K arc magmas: evidence from Egmont Volcano, North Island, New Zealand. Journal of Petrology. 40:167–197.
Procter JN, Cronin SJ, Platz T, Patra A, Dalbey K, Sheridan M, Neall V. 2010. Mapping Block-and-ash flow hazards based on Titan2D simulations; a case study from Mt Taranaki, New Zealand. Natural Hazards. 53:483–501.
Procter JN, Cronin SJ, Zernack AV. 2009. Landscape and Sedimentary Response to Catastrophic Debris Avalanches, Western Taranaki, New Zealand, Sedimentary. Geology. 220:271–287.
Procter JN, Zernack AV, Cronin SJ. 2020. Computer simulation of a volcanic debris avalanche from Mt Taranaki, New Zealand. In: Roverato M, Dufresne A, Procter J, editors. Volcanic Debris Avalanches: from Collapse to Hazard. Cham: Springer Book Series Advances in Volcanology; p. 281–310.
Pyle DM. 2000. Sizes of volcanic eruptions. In: Sigurdsson H, Houghton BF, McNutt SR, Rymer H, Stix J, editor. Encyclopedia of Volcanoes. San Diego, California: Academic Press; p. 263–269.
Reyners M. 1983. Lateral segmentation of the subducted plate at the Hikurangi margin, New Zealand: seismological evidence. Tectonophysics. 96:203–223.
Reyners M, Eberhart-Phillips D, Bannister S. 2011. Tracking repeated subduction of the Hikurangi Plateau beneath New Zealand. Earth and Planetary Science Letters. 311:165–171.
Reyners M, Eberhart-Phillips D, Stewart G, Nishimura Y. 2006. Imaging subduction from the trench to 300 km depth beneath the central North Island, New Zealand, with Vp and Vp/Vs. Geophysical Journal International. 165:565–583.
Roverarto M, Cronin SJ, Procter J, Capra L. 2014. Textural features indicate the transport and emplacement of the >7 km3 Pungarehu debris avalanche deposit, Mt. Taranaki, New Zealand. Geological Society of America Bulletin. 127(1-2):3–18.
Salmon ML, Stern TA, Savage MK. 2011. A major step in the continental Moho and its geodynamic consequences: The Taranaki-Ruapehu line, New Zealand. Geophysical Journal International. 186:32–44.
Sandiford A, Alloway B, Shane P. 2001. A 28000–6600 cal yr record of local and distal volcanism preserved in a paleolake, Auckland, New Zealand. New Zealand Journal of Geology and Geophysics. 44(2):323–336.
Shane P. 2005. Towards a comprehensive distal andesitic tephrostratigraphic framework for New Zealand based on eruptions from Egmont volcano. Journal of Quaternary Science. 20:45–57.
Sherburn S, White RS. 2005. Crustal seismicity in Taranaki, New Zealand using accurate hypocentres from a dense network. Geophysical Journal International. 162:494–506.

Sherburn S, White RS. 2006. Tectonics of the Taranaki region, New Zealand: earthquake focal mechanisms and stress axes. New Zealand Journal of Geology and Geophysics. 49:269–279.
Sherburn S, White RS, Chadwick M. 2006. Three-dimensional tomographic imaging of the Taranaki volcanoes, New Zealand. Geophysical Journal International. 166:957–969.
Siebert L, Glicken H, Ui T. 1987. Volcanic hazards from Bezymianny- and Bandai-type eruptions. Bulletin of Volcanology. 49:435–459.
Stern TA, Holt WE. 1994. Platform subsidence behind an active subduction zone. Nature. 368:233–236.
Stern TA, Houseman GA, Salmon ML, Evans L. 2013. Instability of a lithospheric step beneath western North Island, New Zealand. Geology. 41:423–426.
Stern TA, Smith EGC, Davey FJ, Muirhead KJ. 1987. Crustal and upper mantle structure of the northwestern North Island, New Zealand, from seismic refraction data. Geophysical Journal International. 91:913–936.
Stern TA, Stratford WR, Salmon ML. 2006. Subduction evolution and mantle dynamics at a continental margin: central North Island, New Zealand. Reviews of Geophysics. 44:RG4002.
Stewart RB, Price RC, Smith IEM. 1996. Evolution of high-K arc magma, Egmont volcano, Taranaki, New Zealand: evidence from mineral chemistry. Journal of Volcanology and Geothermal Research. 74:275–295.
Sun S-S, McDonough WF. 1989. Chemical and isotopic systematics of oceanic basalts: implications for mantle composition and processes. In: Saunders AD, Norry MJ, editor. Magmatism in the Ocean Basins. Geological Society. London: Special Publication 42; p. 313–345.
Tatsumi Y, Eggins S. 1995. Subduction Zone Magmatism. Oxford: Blackwell Science.
Torres-Orozco R, Cronin SJ, Damaschke M, Pardo N. 2017. Diverse dynamics of Holocene mafic-intermediate Plinian eruptions at Mt. Taranaki (Egmont), New Zealand. Bulletin of Volcanology. 79(11):Art. No. 76.
Torres-Orozco R, Cronin SJ, Pardo N, Palmer AS. 2017. New insights into Holocene eruption episodes from proximal deposit sequences at Mt. Taranaki (Egmont), New Zealand. Bulletin of Volcanology. 79(1):Art. No. 3.
Torres-Orozco R, Cronin SJ, Pardo N, Palmer AS. 2018. Volcanic hazard scenarios for multiphase andesitic Plinian eruptions from lithostratigraphy: Insights into pyroclastic density current diversity at Mount Taranaki, New Zealand. Geological Society of America Bulletin. 130(9-10):1645–1663.
Townsend D, Nicol A, Mouslopoulou V, Begg JG, Beetham R, Clark D, Giba M, Heron D, Lukovic B, McPherson A, et al. 2010. Palaeoearthquake histories across a normal fault system in the southwest Taranaki Peninsula, New Zealand. New Zealand Journal of Geology and Geophysics. 53(4):375–394.
Turner GM, Alloway BV, Dixon BJ, Atkins CB. 2018. Thermal history of volcanic debris flow deposits on the eastern flanks of Mt. Taranaki, New Zealand: Implications for future hazards. Journal of Volcanology and Geothermal Research. 353:55–67.
Turner M, Bebbington M, Cronin SJ, Stewart RB. 2009. Merging Eruption Datasets: Towards an Integrated Holocene Eruptive Record of Mt Taranaki, New Zealand. Bulletin of Volcanology. 71:903–918.
Turner MB, Cronin SJ, Bebbington MS, Smith IEM, Stewart RB. 2011a. Integrating records of explosive and effusive activity from proximal and distal sequences: Mt. Taranaki, New Zealand. Quaternary International. 246:364–373.
Turner MB, Cronin SJ, Bebbington M, Smith IEM, Stewart RB. 2011b. Relating magma composition to eruption variability at andesitic volcanoes: A case study from Mount Taranaki, New Zealand. Geological Society of America Bulletin. 123:2005–2015.
Turner MB, Cronin SJ, Smith IEM, Stewart RB, Neall VE. 2008a. Eruption episodes and magma recharge events in andesitic systems; Mt Taranaki, New Zealand. Journal of Volcanology and Geothermal Research. 177:1063–1076.
Turner MB, Cronin SJ, Smith IEM, Bebbington M, Stewart RB. 2008b. Using titanomagnetite textures to elucidate volcanic eruption histories. Geology. 36:31–34.
Turner MB, Cronin SJ, Bebbington MS, Platz T. 2008c. Developing a probabilistic eruption forecast for dormant volcanoes; a case study from Mt Taranaki, New Zealand. Bulletin of Volcanology. 70:507–515.
Ui T, Kawachi S, Neall VE. 1986. Fragmentation of debris avalanche material during flowage–evidence from the Pungarehu Formation, Mount Egmont, New Zealand. Journal of Volcanology and Geothermal Research. 27:255–264.
Wallace LM, Beavan J, McCaffrey R, Darby D. 2004. Subduction zone coupling and tectonic block rotations in the North Island, New Zealand. Journal of Geophysical Research. 109:B12406.
Wang T, Bebbington M. 2012. Estimating the likelihood of an eruption from a volcano with missing onsets in its record. Journal of Volcanology and Geothermal Research. 243-244:14–23.
Zernack AV. 2020. Volcanic debris-avalanche deposits in the context of volcaniclastic ring plain successions - A case study from Mt. Taranaki. In: Roverato M, Dufresne A, Procter J, editors. Volcanic Debris Avalanches: from Collapse to Hazard. Cham: Springer Book Series Advances in Volcanology; p. 211–254.
Zernack AV, Cronin SJ, Bebbington MS, Price RC, Smith IEM, Stewart RB, Procter JN. 2012. Forecasting catastrophic stratovolcano collapse: a model based on Mount Taranaki, New Zealand. Geology. 40:983–986.
Zernack AV, Cronin SJ, Neall VE, Procter JN. 2011. A medial to distal volcaniclastic record of an andesitic stratovolcano: detailed stratigraphy of the ring-plain succession of south-west Taranaki, New Zealand. International Journal of Earth Sciences. 100:1937–1966.
Zernack AV, Price RC, Smith IEM, Cronin SJ, Stewart RB. 2012. Temporal evolution of a high-k andesitic magmatic system: Taranaki Volcano, New Zealand. Journal of Petrology. 53:325–363.
Zernack A, Procter J, Cronin SJ. 2009. Sedimentary signatures of cyclic growth and destruction of stratovolcanoes: a case study from Mt. Taranaki, New Zealand. Sedimentary Geology. 220:288–305.
Zorn EU, Rowe MC, Cronin SJ, Ryan AG, Kennedy LA, Russell JK. 2018. Influence of porosity and groundmass crystallinity on dome rock strength: a case study from Mt. Taranaki, New Zealand. Bulletin of Volcanology. 80 (4):Art. No. 35.